SEISMIC ANALYSIS AND RISK ASSESSMENT OF WIND TURBINES

by

Seyedeh Mahta Zakaria

B.S., Civil Engineering, Imam Khomeini International University, 2010

Submitted to the Institute for Graduate Studies in
Science and Engineering in partial fulfillment of
the requirements for the degree of
Master of Science

Graduate Program in Civil Engineering

Boğaziçi University

2015

SEISMIC ANALYSIS AND RISK ASSESSMENT OF WIND TURBINES

APPROVED BY:

Assoc. Prof. Hilmi Lus .....
(Thesis Supervisor)

Assoc. Prof. Serdar Soyöz .....

Assoc. Prof. Çetin Yilmaz .....

DATE OF APPROVAL: 1/22/2015

ACKNOWLEDGEMENTS

I cannot find words to express my gratitude to my beloved parents, Parvaneh and Faroogh Zakaria. If it was not for their great sacrifices, love and support, I would have never been able to finish this work and accomplish any of the things that I have until now.

It is with immense gratitude that I acknowledge the support and help of my thesis supervisor Professor Luş. Without his guidance and persistent help this dissertation would not have been possible.

In addition I would like to thank Professor Güler. His kind assistance with regards to my scholarship paved the way through my studies.

I owe my deepest gratitude to my thesis committee members, especially Professor Soyöz who has also been a great teacher to me and without his dedication and effort I would not have been able to finish this work.

I wish to thank my dear friend Sina Parsnejad. He was always present, in good times and bad times. He always encouraged me, believed in me when I did not even believe in myself and helped me through difficult times.

I would like to thank my dear friend Ata Sarrafi, his friendship and his assistance meant a lot along the way.

I would also like to thank Ekin Özer, who had the patience to go through my research and his kind comments gave me the self-confidence that I needed.

ABSTRACT

SEISMIC ANALYSIS AND RISK ASSESSMENT OF WIND TURBINES

The seismic analyses of two different sizes of wind turbines are investigated in this thesis. The first turbine is a relatively short wind turbine previously subjected to a shake table test. The main objective of this part is to evaluate the accuracy of the finite element model based on the experimental results. Effects of adding the blades to the FEM are investigated. The effects of a detailed model are observed on higher natural frequencies of the structure; however, for this case, those frequencies do not fall into a critical range with regards to the tower's seismic response. The structure is then subjected to a magnified ground motion and nonlinear time history analysis is conducted in order to observe its failure modes. The wind turbine tower is observed to buckle in the vicinity of the lower joint of the tower. The second wind turbine is a modern wind turbine currently operating in one of the campuses of Boğaziçi University. A detailed finite element model is constructed using available information such as the mass distribution. The structure is analyzed using nonlinear time history analyses under earthquakes selected from the Los Angeles, California earthquake suit. The turbine tower is observed to buckle around the areas where there is a thickness change in the wall thickness; however, the level of seismic motion that leads to such failures is significantly high. The base moment demands calculated on the surface of the foundation are significant, and there is a possibility that seismic loads may govern design.

ÖZET

RÜZGÂR TÜRBİNLERİNİN DEPREM ÇÖZÜMLEMESİ VE DEPREM RİSKİ DEGERLENDİRMESİ

Bu tez kapsamında iki farklı rüzgâr türbininin deprem davranışı incelenmektedir. Türbinlerden ilki, daha önce üzerinde sarsma deneyleri gerçekleştirilmiş görece kısa bir rüzgâr türbinidir. Bu incelemenin temel amacı, sonlu elemanlar modelinin geçerliğini deney verileri ışığında değerlendirebilmektir. Sonlu elemanlar modeline rüzgâr kanatlarını eklemenin etkileri üzerinde durulmuştur. Ayrıntılı modelin etkileri yapının yüksek modlarında kendini hissettirmektedir; bununla birlikte, bu durumda söz konusu frekanslar yapının deprem davranışını belirleyen kritik aralıkta bulunmamaktadır. Yapı daha sonra büyütülmüş deprem kayıtları etkisinde, zaman tanım alanında doğrusaldışı çözümleme ile incelenmiş ve göçme modları tespit edilmeye çalışılmıştır. Rüzgâr türbininin kulesinde alt uç yakınlarında burkulma gözlenmiştir. Ele alınan ikinci türbin, Boğaziçi Üniversitesi bünyesinde çalışan modern bir rüzgâr türbinidir. Bu durumda var olan kütle dağılımı bilgisi gibi verilere dayanarak ayrıntılı bir sonlu elemanlar modeli kurulmuştur. Yapı, Los Angeles, California deprem topluluğu arasından seçilen deprem kayıtları etkisinde, zaman tanım alanında doğrusaldışı çözümleme ile incelenmiştir. Türbin kulesinin, duvar kalınlığının değiştiği bölge çevresinde burkulduğu gözlenmiştir; bununla birlikte, böylesi göçmelere yol açan deprem hareketleri oldukça şiddetlidir. Temel üst yüzeyinde hesaplanan taban momentleri dikkate değer olup, deprem yüklerinin tasarımda belirleyici olabilmesinin mümkün olduğu anlaşılmıştır.

TABLE OF CONTENTS

ACKNOWLEDGEMENTS iii
ABSTRACT iv
ÖZET v
LIST OF FIGURES viii
LIST OF TABLES xiv
LIST OF SYMBOLS xv
LIST OF ACRONYMS/ABBREVIATIONS xvii
1. INTRODUCTION AND BACKGROUND 1
1.1. Introduction 1
1.2. An Introduction to Wind Turbines 2
1.2.1. Types of Wind Turbines 2
1.2.2. Components of a Wind Turbine 4
1.2.3. Operational States of a Wind Turbine 4
1.2.4. Wind Farms 5
1.3. Literature Review 6
1.3.1. Existing Codes and Standards 6
1.3.2. Research Studies 7
1.4. Overview of Thesis 11
2. DEVELOPEMENT OF THE FINITE ELEMENT MODEL AND THE VALIDATION 12
2.1. Geometry and Material Properties of Nordtank 65 kW Wind Turbine . 12
2.1.1. Tower 13
2.1.2. Nacelle 14
2.1.3. Rotor 15
2.2. Choice of Elements 15
2.3. Frequency Extraction and Modal Analysis 17
2.3.1. Mode Shapes 17
2.3.2. Comparison Between the Natural Frequencies 19

2.4. Damping 21
2.5. Modal Analysis and Validation of the Time-history Results 21
2.5.1. Earthquake Records 21
2.5.2. Modal Dynamic Analysis Results and Comparisons with the Shake-table Test 23
2.6. A Basic Study on the Importance of Adding the Blades to the Finite Element Model 26
2.6.1. Earthquake Records 26
2.6.2. Nonlinear Time-history Analysis with Direct Integration Method 26
2.6.3. Damping 27
2.6.4. The Method of Subjecting the Structure to Ground Motion . . 28
2.6.5. Simplified FEM vs. Detailed FEM 28
2.6.6. Nonlinear Time-history Analysis 32
3. SEISMIC ANALYSIS OF THE BÜRES 900 KW WIND TURBINE 34
3.1. Dimensions and Material Properties of the BÜRES 900 kW Wind Turbine 34
3.2. Finite Element Model and Natural Frequencies 37
3.3. Damping 39
3.4. Ground Motion Inputs 40
3.5. Nonlinear Time-history Analysis 43
3.5.1. Comparison Between the Two Tower Sections 43
3.6. Time-history Results of the Four Chosen Earthquakes 45
3.6.1. Time-history Results of Landers Earthquake 45
3.6.2. Time-history Results of Imperial Valley 1940 Earthquake 46
3.6.3. Time-history Results of Imperial Valley 1979 Earthquake 47
3.6.4. Comparison between the Peak Results and Demand 48
4. CONCLUSIONS AND FUTURE WORK 49
4.1. Conclusions 49
4.2. Future Work 49
APPENDIX A: Time-History Results of BÜRES Wind Turbine 51
APPENDIX B: Response Spectras of the Ground Motions 60
REFERENCES 63

LIST OF FIGURES

Figure 1.1. Horizontal–axis wind turbine (HAW). 3

Figure 1.2. Vertical–axis wind turbine (VAW). 3

Figure 1.3. Parts of a wind turbine. 4

Figure 1.4. Cut–in and cut–out speed of the 65 kW wind turbine analyzed by Prowell et al., [1]. 5

Figure 2.1. Stress-strain curve of 65 kW wind turbine [2]. 14

Figure 2.2. Finite element model of Nordtank 65kW wind turbine in this study. 16

Figure 2.3. Experimentally and numerically identified lateral modes of the tower as given in [3]. 17

Figure 2.4. First three fore-aft mode shapes obtained in the current study. . . 18

Figure 2.5. First three side-to-side mode shapes obtained in the current study. 18

Figure 2.6. Fore-aft mode shapes for the lumped mass model. 20

Figure 2.7. Side-to-side mode shapes for the lumped mass model. 20

Figure 2.8. Landers earthquake ground acceleration time-history. 22

Figure 2.9. Landers earthquake response spectra. 23

Figure 2.10. Nordtank 65 kW wind turbine: sensor locations [1]. 24

Figure 2.11. Acceleration time-history recorded during the shake-table test [3]. 25

Figure 2.12. Acceleration time-history results obtained in the current study. . . 25

Figure 2.13. Mass contribution of the detailed model between the modes. . . . 29

Figure 2.14. With blades vs. without blades, SS direction, Landers ground motion. 30

Figure 2.15. With blades vs. without blades, FA direction, Landers ground motion. 30

Figure 2.16. With blades vs. without blades, SS direction, Imperial Valley ground motion. 31

Figure 2.17. With blades Vs. without blades, SS direction, Palm Springs. . . . 32

Figure 2.18. With blades Vs. without blades, FA direction, Palm Springs. . . . 32

Figure 2.19. Buckling of the 65kW wind turbine tower. 33

Figure 3.1. 900 kW wind turbine tower and its dimensions. 36

Figure 3.2. 900 kW wind turbine figure. 36

Figure 3.3. Schematic sketch of the cross section of the blade. 37

Figure 3.4. Finite element model of BURES wind turbine. 38

Figure 3.5. SS mode shapes. 38

Figure 3.6. FA mode shapes. 39

Figure 3.7. Comparison between the free vibration of modal dynamics and direct integration method. 40

Figure 3.8. Response spectra of selected ground motions vs. the design spectrum. 41

Figure 3.9. Response spectra of the amplified (scaled to 300%) ground motions vs. the design spectrum. 41

Figure 3.10. Mean spectrum. 42

Figure 3.11. Mass contributions of the modes in the SS direction. 43

Figure 3.12. Failure modes. 44

Figure 3.13. Top displacement in the horizontal x and z directions. 45

Figure 3.14. Top displacement in the horizontal x direction due to the amplified Imperial Valley 1940 record. 46

Figure 3.15. Top displacement in the horizontal z direction due to the amplified Imperial Valley 1940 record. 46

Figure 3.16. Top displacement in the horizontal x direction doe to the amplified Imperial Valley 1979 record. 47

Figure 3.17. Top displacement in the horizontal z direction due to the amplified Imperial Valley 1979 record. 47

Figure A.1. Top acceleration in the horizontal x direction due to the amplified Landers record. 51

Figure A.2. Top acceleration in the horizontal z direction due to the amplified Landers record. 51

Figure A.3. Base shear in the horizontal x direction due to the amplified Landers record. 51

Figure A.4. Reaction force in the vertical direction due to the amplified Landers record. 52

Figure A.5. Base shear in the horizontal z direction due to the amplified Landers record. 52

Figure A.6. Base moment with respect to the horizontal x axis due to the amplified Landers record. 52

Figure A.7. Base moment with respect to the vertical axis due to the amplified Landers record. 53

Figure A.8. Base moment with respect to the horizontal z axis due to the amplified Landers record. 53

Figure A.9. Top acceleration in the horizontal x direction due to the amplified Imperial Valley 1940 record. 53

Figure A.10. Top acceleration in the vertical y direction due to the amplified Imperial Valley 1940 record. 54

Figure A.11. Top acceleration in the horizontal z direction due to the amplified Imperial Valley 1940 record. 54

Figure A.12. Base shear in the horizontal x direction due to the amplified Imperial Valley 1940 record. 54

Figure A.13. Reaction force in the vertical direction due to the amplified Imperial Valley 1940 record. 55

Figure A.14. Base shear in the horizontal z direction due to the amplified Imperial Valley 1940 record. 55

Figure A.15. Base moment with respect to the horizontal x axis due to the amplified Imperial Valley 1940 record. 55

Figure A.16. Base moment with respect to the vertical y axis due to the amplified Imperial Valley 1940 record. 56

Figure A.17. Base moment with respect to the horizontal z axis due to the amplified Imperial Valley 1940 record. 56

Figure A.18. Top acceleration in horizontal x direction due to the amplified Imperial Valley 1979 record. 56

Figure A.19. Top acceleration in the horizontal z direction due to the amplified Imperial Valley 1979 record. 57

Figure A.20. Base shear in the horizontal x direction due the amplified Imperial Valley 1979 record. 57

Figure A.21. Reaction force in the vertical direction due the amplified Imperial Valley 1979 record. 57

Figure A.22. Base shear in the horizontal z direction due the amplified Imperial Valley 1979 record. 58

Figure A.23. Base moment with respect to the horizontal x axis due the amplified Imperial Valley 1979 record. 58

Figure A.24. Base moment with respect to the vertical y axis due the amplified Imperial Valley 1979 record. 58

Figure A.25. Base moment with respect to the horizontal z axis due the amplified Imperial Valley 1979 record. 59

Figure B.1. Response spectra of the Imperial Valley record, N-S direction. . . 60

Figure B.2. Response spectra of the Imperial Valley record, vertical direction. 60

Figure B.3. Response spectra of the Imperial Valley record, E-W direction. . . 61

Figure B.4. Response spectra of the N.Palm Springs record, E-W direction. . . 61

Figure B.5. Response spectra of the N. Palm Springs record, vertical direction. 62

Figure B.6. Response spectra of the N. Palm Springs record, N-S direction. . . 62

LIST OF TABLES

Table 2.1. Properties of the 65 kW wind turbine [3]. 13

Table 2.2. Comparison of the natural frequencies obtained in the current study with those given by [3]. 19

Table 2.3. Obtained modal damping ratios by Prowell et al., [4]. 21

Table 2.4. Landers Earthquake specifications [5]. 22

Table 2.5. Information about the four chosen earthquake records. 26

Table 3.1. 900 kW wind turbine's technical specifications. 35

Table 3.2. Specifications of the ground motions. 40

Table 3.3. Comparisons between the base shear and the base moment for amplified ground motion records. 48

LIST OF SYMBOLS

a	Acceleration
$A1$	Acceleration in SS direction
$A2$	Acceleration in vertical direction
$A3$	Acceleration in FA direction
$\left[C\right]$	Damping matrix
E	Young's Modulus
f	Natural frequency of the structure
Fx	Base shear in side to side direction
Fy	Vertical reaction force
Fz	Base shear in fore-aft direction
GW	Gigawatt
$\left[K\right]$	Stiffness matrix
kW	Kilowatt
m	Meter
$\left[M\right]$	Mass matrix
mm	Millimeters
MW	Megawatt
Mx	Base moment with respect to x axis (SS)
My	Base moment with respect to y axis (SS)
Mz	Base moment with respect to z axis (FA)
N	Newoton
Pa	Paskal
s	Second
Sa	Spectral acceleration
T	Natural period of the structure
u	Displacement
U1	Displacement in SS direction
U2	Displacement in vertical direction

U3	Displacement in FA direction
u_g	Ground displacement
$\left\{u(t)\right\}$	Absolute or relative displacement to the ground
V	Velocity
ζ	Modal Damping ratio
α	Rayleigh damping coefficient
β	Rayleigh damping coefficient
ω_i	Natural frequency of the ith mode
ϵ	Strain
ϵ_{nom}	Nominal strain
σ	Stress
σ_{nom}	Nominal stress

LIST OF ACRONYMS/ABBREVIATIONS

ASCE	American Society of Civil Engineering
AWE	American Wind Energy Association
DOF	Degree of freedom
FA	Fore-Aft direction of the wind turbine
FAST	Fatigue, Aerodynamics, Structures and Turbulence
FEM	Finite element model
GL	Germanischer Lloyd
HAW	Horizontal axis wind turbine
LHPOST	Large High Performance Outdoor Shake Table
NREL	National Renewable Energy Laboratory
Opensees	Open System for Earthquake Engineering Simulation
PGA	Peak ground acceleration
RMS	Root mean-squared acceleration
RPM	Revolutions per minute
SDOF	Single degree of freedom
SS	Side to side, lateral direction of the wind turbine
TÜREB	Türkiye Rüzgar Enerjisi Birligi
UCSD	University of California, San Diego
VAW	Vertical axis wind turbine

1. INTRODUCTION AND BACKGROUND

1.1. Introduction

The increasing demand for renewable energy has had a noticeable impact on the improvement of the structures harvesting these sources. Wind energy in one of the clean sources and wind turbines are the primary structures for harvesting wind energy. There have been several studies regarding the failure and fatigue issues with wind turbine blades and other equipment. There are also many studies considering the response of these structures under wind and operational loads.

Recently the use of these structures in seismically hazardous regions has increased. Countries such as United States and China are currently producing a noticeable amount of electricity from wind energy. Turkey also has a significant potential for harvesting wind energy. According to a report by the European Wind Energy Association [6], Turkey has one of the largest wind energy pipelines in Europe with operational, under construction and planned projects adding up to 11 GW. The country's substantial wind potential, estimated around 48 GW, is expected to attract significant investment. The highest wind speeds are along the Aegean, Marmara, and eastern Mediterranean shores, reaching 10 m/s on average [7]. These areas are mostly located on regions with high seismic hazard. There is an apparent need for a thorough investigation on how these structures would behave in case of a probable earthquake. What makes this investigation more vital is the fact that most of the building codes, including the current Turkish code [8], and wind turbine guidelines do not fully address the essential information regarding the design of these structures under seismic loading. Adding to the problem is the availability of real life data, as there are not so many experiments or physical evidence available regarding the seismic response and failure of wind turbines; the performance requirements on these structures may be expected to be more stringent than those on more "ordinary" structures in that such turbines are may be expected to remain fully operational after an earthquake to provide uninterrupted power. A factor that may exacerbate the problem is the ex-

pected correlation under operational conditions: wind farms generally comprise many turbines with identical circumstances and therefore an earthquake may damage many of such turbines, leading to a huge financial loss.

1.2. An Introduction to Wind Turbines

A wind turbine is a machine which converts kinetic energy into mechanical energy. If the machine uses the mechanical energy directly, such as to pump, then the machine is called a windmill. If the mechanical energy is converted to electricity, it is called wind turbine.

1.2.1. Types of Wind Turbines

There are two different types of wind turbines: Horizontal–axis wind turbines (Figure 1.1) and vertical–axis wind turbines (Figure 1.2). A horizontal axis wind turbine has its blades rotating on an axis parallel to the ground. A vertical axis wind turbine has its blades rotating on an axis perpendicular to the ground. Both designs have unique advantages and disadvantages. Horizontal axis wind turbines are more commonly used in electricity production, especially for industrial purposes, mostly because they produce electricity more effectively [9].

Vertical axis wind turbines are usually used for more residential purposes, as they are ideal for installation at locations for which wind conditions are not consistent. Moreover, they have a Low production cost as compared to horizontal axis wind turbine. Their installation and transportation is also simpler compared to horizontal axis wind turbines.

In this study, the seismic response of horizontal axis wind turbines will be evaluated, as their are more vulnerable towards the seismic hazard, and their failure can cause a more severe financial loss.



Figure 1.1. Horizontal–axis wind turbine (HAW).



Figure 1.2. Vertical–axis wind turbine (VAW).

1.2.2. Components of a Wind Turbine

Each wind turbine consists of three main components indicated on Figure 1.3: The tower, the nacelle and the rotor. The nacelle contains the key components of the wind turbine, including the gearbox and the generator. The rotor blades capture the wind energy and transfer it to the rotor hub. The tower carries the nacelle and the rotor. In general, having a high tower is beneficial since the wind speed increases with the height.

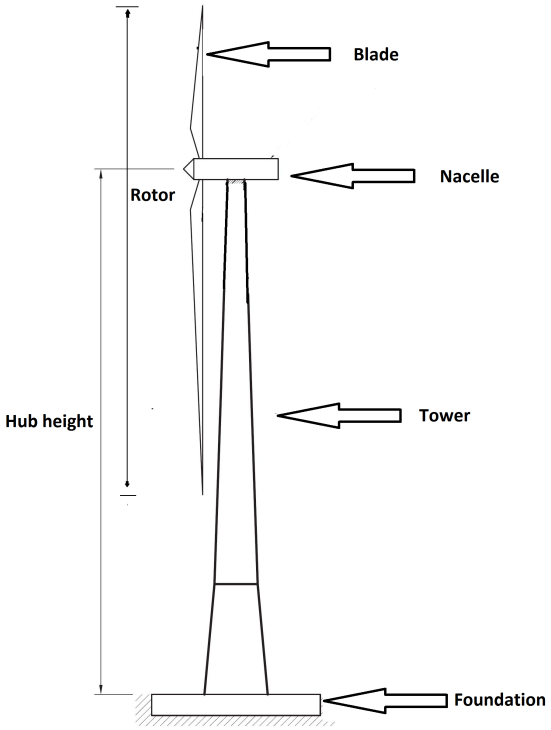

Figure 1.3. Parts of a wind turbine.

1.2.3. Operational States of a Wind Turbine

Wind turbines have two operational states denoted as operating and parked. The turbine is parked in two circumstances: when the wind speed is below a certain level, and when it is greater than a certain threshold. These levels are called the cut–in and the cut-out wind speeds [10]; Figure 1.4 shows the cut–in and the cut–out speed of

the 65 kW wind turbine analyzed by UCSD [1]. There is also an emergency shutdown system in case of an unexpected event such as an earthquake or a sudden gust. There are sensors on the structure which will automatically signal the emergency break when the vibration of the structure increases to a limit.

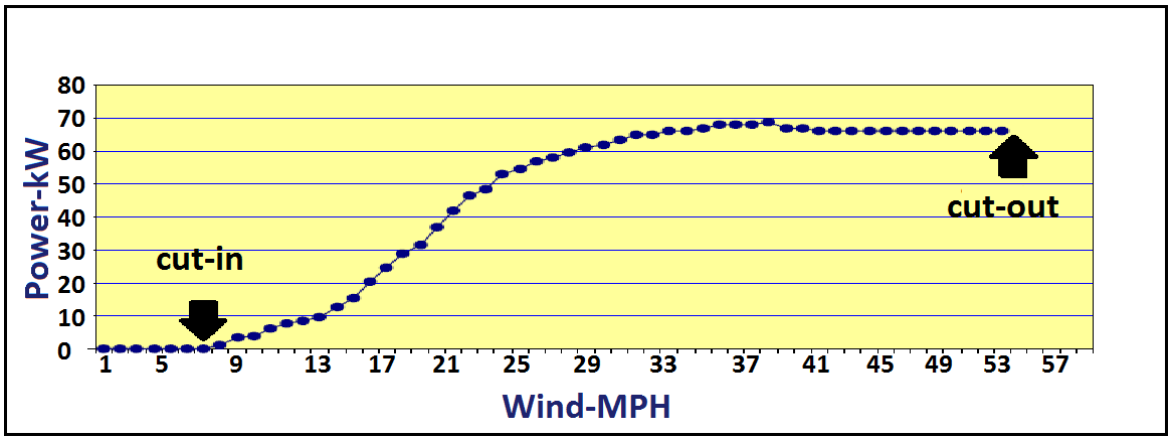

Figure 1.4. Cut–in and cut–out speed of the 65 kW wind turbine analyzed by Prowell et al., [1].

1.2.4. Wind Farms

A wind farm is an area where multiple wind turbines are installed to generate electricity. Wind farms can be on the ground or in the sea. Those on the ground are called onshore wind farms whereas those in the sea are known as offshore wind farms. The wind farms can consist of a few dozens to several hundreds of wind turbines. Such farms may especially be susceptible to earthquake damage, for the proximity of the towers and in most instances their identical design may lead to correlated damage. The risk management of such farms, therefore, is an important problem in and of itself, and the analyses presented in this study may be expected to serve as a first step in that direction.

1.3. Literature Review

Significant progress has been made in understanding the response of wind turbines under wind loads. Most of the studies addressing this subject have focused on issues such as fatigue, lifetime and failure of wind turbines. The target economical life time of a wind turbine is currently estimated as 20 years [11], and this span is mostly governed by the lifetime of the blades. The literature on the seismic response of these structures, however, is not as vastly developed as those on the aforementioned topics. The literature review presented in this section is aimed at providing an understanding of the current state of research on the study of seismic response of wind turbines.

1.3.1. Existing Codes and Standards

There are three main standards which provide guidance for the seismic design of wind turbines. *Guideline for the design of wind turbines* [12]; *guideline for the certification of wind turbines* [13], and American Society of Civil Engineering and American Wind Energy Association's ASCE-AWEA guideline [14, 15]. Other building codes such as Turkish Earthquake Code [8] do not explicitly address wind turbines.

Guideline for the design of wind turbines [12] provides general information regarding the design of wind turbine structures in seismically hazardous regions. In this guideline it is suggested to use a simplified model in order to analyze a wind turbine under seismic loads. It is said that the nacelle and the rotor can be considered as a lumped mass on the top, with the weight equal to the total weight of the nacelle, the rotor and $\frac{1}{4}$ of the tower mass. It is suggested that the design response spectrum can be used in order to determine the seismic loads on the tower. There is no recommendation regarding the appropriate level of damping. In the absence of specific guidance regarding the interpretation of spectral accelerations, it is assumed that the procedures specified in general building codes will be employed.

ASCE-AWEA [14, 15] is the most recent guideline which provides particular information regarding the seismic design of wind turbines. In this guideline, it has

been stated that seismic ground motion values should be determined per ASCE-7-05, Section 11.4, or the site specific ground motion procedure set forth in ASCE7-05, Chapter 21. It has also been mentioned that in case of a parked wind turbine the spectral response acceleration parameter should be based on 1 percent damped values. The guideline has also introduced an adjustment factor in order to adjust the spectral response acceleration from 5 percent damping to the target value of damping. Another important factor that has been mentioned in this code is related to the operational state of wind turbines after a design level earthquake. As mentioned before, the guideline suggests that the earthquake design should be in accordance with local building codes. However, it is worth mentioning that local building codes do not ensure that the structure is operational after a design level earthquake. Although this design level may not harm any human lives, the level of damage is important to wind farm owners. Therefore a clear distinction should be made between the required minimum performance objectives of the local building code (life–safety) versus that of any supplementary, project-specific contractual agreement. In this code there is also a proposed load combination to address an operational state and an earthquake event jointly.

1.3.2. Research Studies

Regarding the seismic analysis of wind turbines there are certain aspects that needs to be investigated. The analysis methods, the damping of the structure, the necessity of a detailed model versus simplified models and the failure modes are the most important issues that have been discussed in previous research on seismic response of wind turbines.

Early studies considering the seismic response of wind turbines use simplified models in order to capture the response. In these studies the nacelle and the rotor are jointly considered as a single lumped mass on the top of the tower. The focus in these cases are mostly on the response of the tower. Bazoes et al., [16] present a finite element model of a prototype 450 kW turbine with a hub height of 38 meters. In this study the tower is modeled in two ways, one that uses beam column elements and

another with more details using shell elements. In both models the nacelle and the rotor are considered as a single lumped mass on the top. Time history analysis of the two models were compared. The models show good agreement. SSI was also considered in this study. The results show that the seismic loading was not the governing load in this study.

A finite element investigation of a 1 MW wind turbine is presented by Lavassas et al., [17]. In this study the authors use the design spectrum provided in Eurocode 3 for a site located in Seismic Zone II. The nacelle and the rotor in this case are also considered as a lumped mass on the top. The authors conclude that the seismic stresses are 60% less than those produced by the extreme wind load.

Ishihara and Sarwar [18] provide a comparison of the performance of simplified models with more detailed models. Their study investigates the seismic demand of two different wind turbines with two different types of modeling. The first method for modeling is the simplified model considering the mass of the rotor and nacelle as a lumped mass on the top of the tower. The second method considers the mass and stiffness of the rotor distributed. It is concluded that both models satisfactorily capture the response of these structures. It is also explained that with the taller wind turbine (2 MW) higher modes have a more significant effect on the seismic response. Therefore, they suggest that for the turbines with a hub height above 60 meters, a detailed model is necessary. Prowell et al., [3] also state a similar matter which will be elaborated shortly.

An investigation was carried out by *Windrad Engineering GmbH* and *Nordex Energy GmbH* [19]. The method of modal approximation was compared with a time-domain approach using the simulation program Flex5 [20]. The main reason for investigating this comparison is because they believe modal approximation is not an adequate method for obtaining design loads, especially the rotor and nacelle loads, as modal approximation ignores any action above the tower top. Thus, any system modes which might take into account the interaction of the tower and the blades are not considered. The results of this investigation suggest that the modal approach is

very conservative for the lower part of the tower [19]. Regarding the machine loads on the nacelle and the rotor, the time-domain method predicts high vertical forces, which are not predicted by the modal approximation method because the vertical component is ignored [19]. Both the time-domain method and the frequency-domain method were deemed to be adequate.

A relatively detailed analysis was conducted in 2010 by Nuta et al., [21]. At the first stage of the analysis, the wind turbine model was validated based on the shake table test [3]. The model showed a good agreement with regards to the first frequencies but it lacked accuracy with regards to the higher modes. Then another model of a modern wind turbine was constructed to capture the seismic response of a taller wind turbine. An incremental dynamic analysis was run and fragility curves were obtained. The structure was based on the Canadian Seismic Code, and according to the results, the probability of failure of these structure in the Canadian environment is very low, such that the wind induced loads govern the design.

A detailed analysis of wind turbines considering the aerodynamic effects needed more detailed modeling tools. Two such tools worth mentioning are GH Bladed and the FAST code. Both were verified by Germanischer Lloyd (GL) [22].

GH Bladed was produced by Garrad Hassan. GH Bladed does not use finite element model in order to analyze the turbine. Instead, it uses limited number of modes to run a modal analysis. The seismic module was added to GH Bladed by Bossanyi [23]. The software is capable of analyzing the wind turbine in time domain considering different levels of damping and subjected to different load combinations.

The FAST code was developed by Jonkman and Buhl [24] and it is maintained by the United States National Renewable Energy Laboratory (NREL). The code uses a combined modal and multi-body dynamics formulation to obtain the dynamic behavior of a wind turbine. Prowell et al., [25] modified the FAST code in order to simulate the seismic load.

Witcher [26] looks into the difference between the two methods of analysis: time domain and frequency domain . The author uses GH Bladed to analyze the wind turbines. The article mentions that the comparisons between frequency and time domain methods have shown surprisingly similar results for operating turbines. The reason is primarily because of the aerodynamic damping experienced by an operating turbine that is close to 5% value used for design spectra. However, a parked turbine experiences a significantly lower damping and building codes did not provide a method for correcting the level of damping at the time. The study also compares the base moment between each analysis. In the parked condition there is a 79% difference between the results obtained via the two methods; however, even the most conservative results are still less than the critical demands for an operating wind turbine, such that the analysis method does not seem to have any bearing on the design.

Researchers from the University of California, San Diego have conducted an extensive experimental and numerical study on the seismic behavior of wind turbines. The seismic response of a 65kW wind turbine was obtained at a large high performance shake table in 2004 [1, 3, 4]. The damping of the structure, along with its natural frequencies, were obtained from the data. The results from the experiments were compared with the response predicted via two models: the simplified model considering the rotor as a lumped mass on the top and a more detailed model considering the blades as beam-column elements. The authors conclude that although the results of the simplified model did not have a noticeable difference with a more detailed model, the inconsistency increases with higher modes. Prowell et al., [4] also introduce two different amounts of damping for the two operational conditions of a wind turbine. During the experiment, it has been observed that aerodynamic damping has a noticeable effect on the damping of the whole structure, increasing it from almost 1% to 5% while operating. The seismic response of the 65kW wind turbine is mostly governed by its first mode; however, the authors argue that with the modern wind turbines the higher modes also fall into the critical range. Therefore, there is a need for a more detailed finite element model.The most extensive part of the study was conducted in 2010 where the seismic response of the wind turbine was obtained both while oper-

ating and while parked. Three different ground inputs given in order to obtain the response of the structure at various points on the tower and the nacelle [19]. The FAST code was also modified in order to give the base motion along with other loads as an input to the code for the analysis of a wind turbine. The results from FAST codes were then validated those obtained from Opensees (*An open source computational platform* [27]).

In a latter study [28], the aerodynamic demands for a 1 MW reference wind turbine is calculated, and it is observed that aerodynamic loads become more necessary as the height of the wind turbine increases.

1.4. Overview of Thesis

In this thesis, the seismic responses of two different sizes of wind turbines will be investigated.

The first of these turbines is the numerical model of the turbine studied in [1]. The aim of this investigation is to get acquainted with the details of numerical modeling and to calibrate the model with real data available from the shake table tests. This investigation will also provide the opportunity to discuss issues such as the choice of numerical integration method, model complexity and damping, cast against the background of real data.

The second turbine is a numerical model of the BÜRES turbine of Boğaziçi University, recently erected at the Kilyos Campus. This is a significantly larger structure than the previous model and builds on the experience obtained via the first investigation. The aim of this part of the study is to determine the possible failure modes and the critical demand thresholds for seismic safety of the turbine.

2. DEVELOPEMENT OF THE FINITE ELEMENT MODEL AND THE VALIDATION

Numerical models are most certainly useful for estimating the response of structures, and in cases of unusual loadings and complex structures for which analytical methods are difficult to employ, they are essential and indispensable. Seismic response of structures is of these more intricate cases; however, in order to be able to rely on the outputs of a numerical model, it is important to validate it.

There are several methods for verifying a numerical model. One method can be the verification of results based on real events, such as the response recorded during a ground motion, also recorded in part or in full. The failure modes of a structure can be observed after the event and compared with those predicted by the numerical model. Experimental results are also a good resource for validating such models, as the prediction results may be compared with those from the controlled experiment.

As for wind turbines, there are not many real life events and observed failures regarding the seismic response of these structures. The most recent and thorough experiment on the behavior of these structures under a seismic excitation was conducted by researchers from the University of California, San Diego [1, 3, 4, 28]. This experiment, henceforth referred to as the UCSD experiment, and the results published by the involved research group, henceforth referred to as the UCSD results, offers a significant opportunity for validating a detailed numerical model of a real wind turbine.

2.1. Geometry and Material Properties of Nordtank 65 kW Wind Turbine

The subject of the UCSD experiment is a Nordtank 65 kW turbine, and some useful information regarding its size, mass, dimensions and material properties have been published [1]. Table 2.1 indicates the mass and dimensions of the structure under consideration. It should be noted that although some structural data is available, there are some additional properties which need to be defined by user.

Table 2.1. Properties of the 65 kW wind turbine [3].

Property	Values
Rated power	65kW
Rated wind speed	11.9 m/s
Operational RMP	45-55 RMP
Rotor diameter	16 m
Tower height	21.9 m
Lower section length	7.9 m
Lower section diameter	2 m
Middle section length	7.9 m
Middle section diameter	1.6 m
Upper section length	7.9
Upper section diameter	1.2 m
Tower wall thickness	6 mm
Rotor hub height	22.6 m
Tower mass	6400 kg
Nacelle mass	2400 kg
Rotor mass with hub	1900 kg

2.1.1. Tower

There is sufficient data available on the dimensions and mass property of the tower, presented in Table 2.1. Based on all the information available, the tower was modeled as a cylindrical shell of steel in this thesis.

In addition to the shake table test, flexural tests have also been performed on the steel tower. The material property of the tower used in this thesis comes from the same experiment. Figure 2.1 is the stress-strain curve of the tower material. In the

numerical analyses herein the true stress-strain curve is employed, which is obtained by modifying the engineering stress-strain curve:

$$\epsilon = \ln(1 + \epsilon_{nom}) \tag{2.1a}$$

$$\sigma = \sigma_{nom}(1 + \epsilon_{nom}) \tag{2.1b}$$

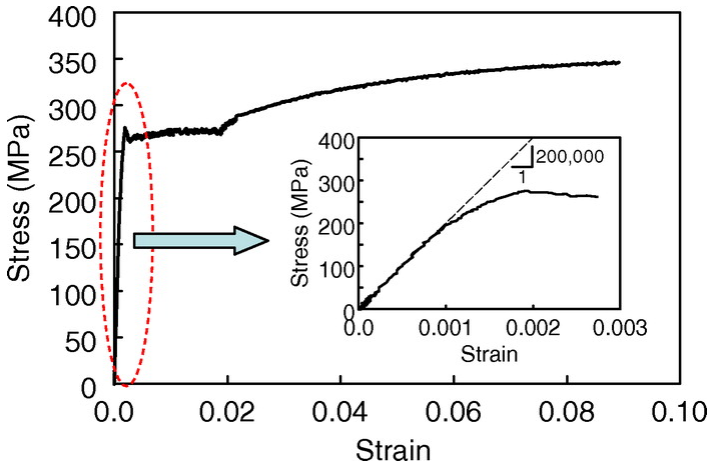

Figure 2.1. Stress-strain curve of 65 kW wind turbine [2].

2.1.2. Nacelle

As for the nacelle, except for the mass, the only available data is its height which can be deduced from the tower height and the hub height. Therefore, the length and width of the nacelle is user-defined, based on some approximate values from the available sketches. The nacelle's size is played with to observe the differences in natural frequencies and time history results. The details of such analysis are presented in this chapter. The total mass is kept consistent with the true mass. Some differences are observed as the size of the nacelle is changed; however, they are too small to be significant. Other material properties of the nacelle, such as its modulus of elasticity, are also user-defined. Nacelle's material was considered as a perfectly elastic material.

2.1.3. Rotor

A wind turbine blade has a complicated geometry including internal stiffeners for which the geometric details and material details are missing. In lack of details, a possible way to model the blades is to consider them as cylindrical elements. The cross section varies along the length similar to the real wind turbine blade. The tip of the blade has a considerably smaller cross section. Since the stiffness and mass distribution is not available, some estimations are needed. The rotor's total mass is 1900 kg [1]; however, the distribution of this mass between the hub and the blades is also important. In this thesis, different mass ratios are considered in order to observe the differences. Although how the mass is distributed has little effect on the first natural frequency of the structure, the higher modes are sensitive to it. A detailed comparison of each distribution will be explained in Section 2.6.5. The final distribution was chosen based on a trial and error method, in the context of the seismic response of the wind turbine. In this thesis, 0.2 times the mass of rotor belongs to the blades . By employing the same ratio to the finite element model here, the results are quite consistent with the UCSD results. In order to match the observed response and natural periods, stiffness is somewhat modified as well. Unfortunately, there is not any certainty regarding the stiffness;however, based on the multiple frequency extractions with different stiffness values considered for the blades, it is believed that in this particular case, the deviation is not that significant, mostly due to the fact that the seismic response of Nordtank 65kW wind turbine is governed by its first modes. Due to the uncertainties regarding the material properties of the blades, their inelastic behavior is not considered the model.

2.2. Choice of Elements

The elements selected for the analyses are 8-node shell elements and 8-node solid elements defined in ABAQUS (Finite-element Computer Code) [29].The tower is represented by 8-node shell elements, which are believed to be able to reflect the tower's behavior. Due to the large diameter-thickness ratio in the tower, it is believed that the behavior of the tower will be similar to a thin shell structure, with a potential for

local buckling. Each node on an element has 6 degrees of freedom (DOF), comprising 3 translational DOFs and 3 rotational DOFs. The element shapes were chosen to be quadratic (S8R5) [30]. These elements are capable of capturing the response of a thin shell when it is curved. Solid elements were chosen for the nacelle. Blades were also modeled with thick shell elements (S4R) [30]. These elements are capable of capturing the response of both thin and thick shell elements. This type of element was intentionally chosen since the thickness of the blade was played with through the whole analysis for mass and stiffness modifications. Figure 2.2 displays the mesh of the finite element model of the wind turbine.

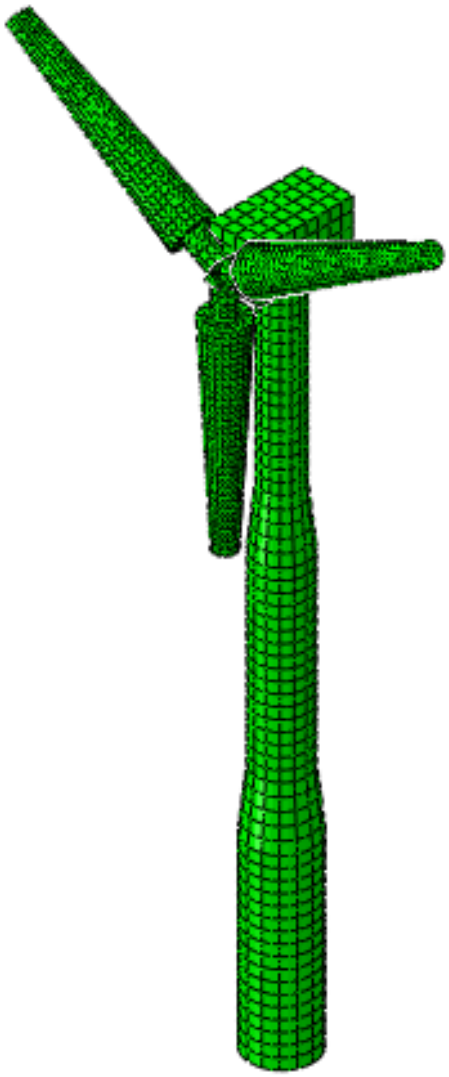

Figure 2.2. Finite element model of Nordtank 65kW wind turbine in this study.

2.3. Frequency Extraction and Modal Analysis

In order to validate the results of the finite element model, several frequency extraction analyses are conducted. The frequencies thus obtained are then compared with those from the series of shake table tests [1, 3, 4].

2.3.1. Mode Shapes

Prowell et al., [3] initially compare the lateral modes of the lumped mass model with those from the experiment. Figure 2.3 displays the experimental and numerical modal properties obtained in [3]. Figures 2.4 and 2.5, are the first three mode shapes in FA and SA direction obtained in the current study respectively.

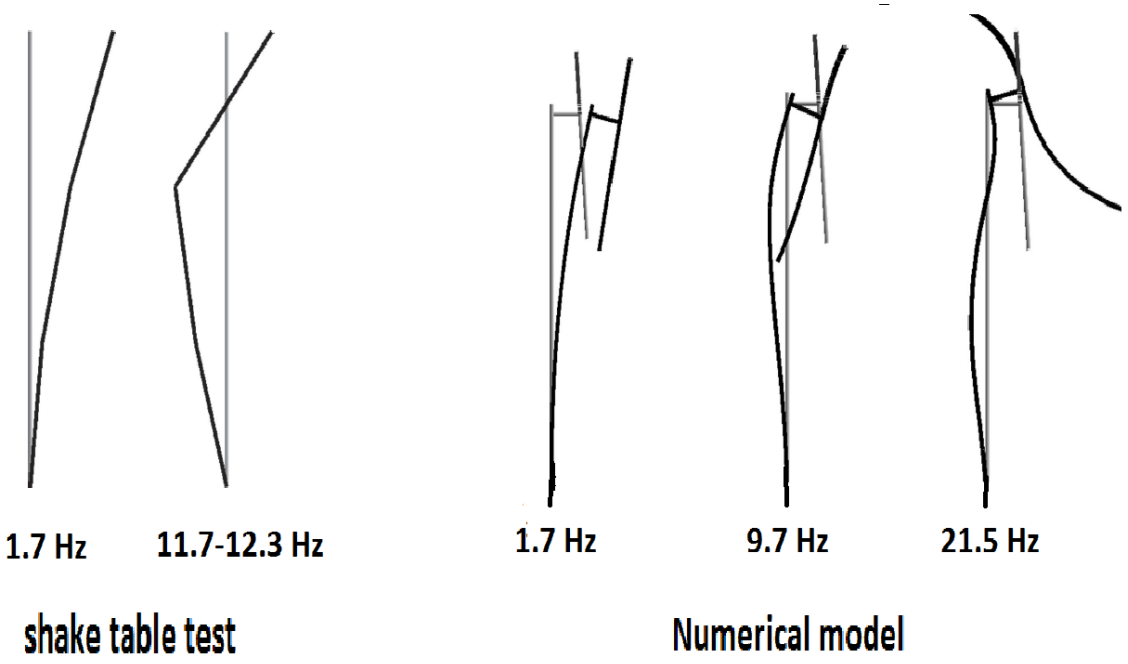

Figure 2.3. Experimentally and numerically identified lateral modes of the tower as given in [3].

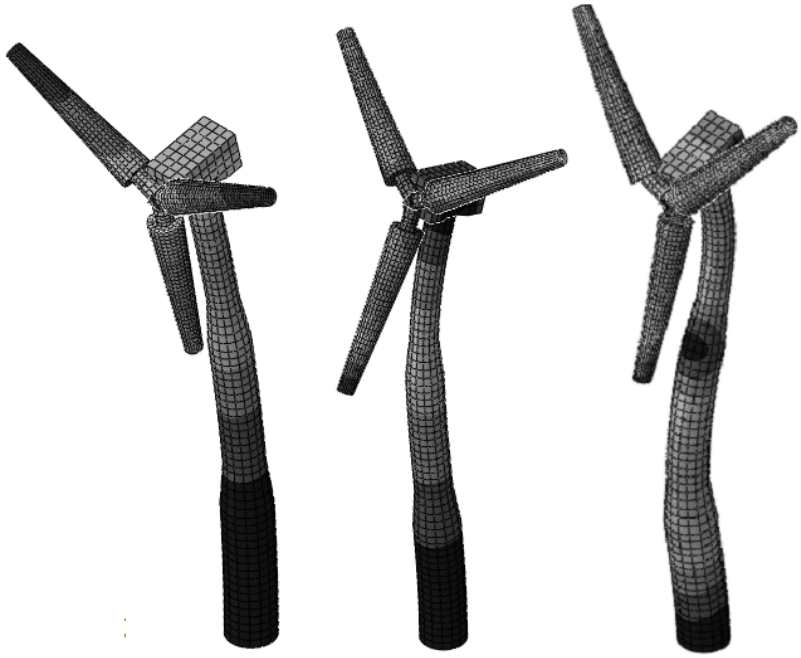

Figure 2.4. First three fore-aft mode shapes obtained in the current study.



Figure 2.5. First three side-to-side mode shapes obtained in the current study.

2.3.2. Comparison Between the Natural Frequencies

The first step to validate the numerical model is to compare the natural frequency results with those obtained from the shake table test and the numerical models developed by Prowell et al., [3]. To this end, two numerical models were created in this study. The first model considers all the structural elements which may effect the seismic response. The second model is a more simplified model, where the mass of the rotor is considered as a lumped mass on top of the tower. Figures 2.6 and 2.7 display the mode shapes of the lumped mass FEM in FA and SS direction respectively. Table 2.2 presents a comparison between the first three modes of the structure both in the SS and the FA directions.

Table 2.2. Comparison of the natural frequencies obtained in the current study with those given by [3].

Mode	Shake table test	Detailed model, [3]	Lumped model, [3]	Detailed model	Lumped model
SS1	1.7 Hz	1.7 Hz	1.7 Hz	1.73 Hz	1.7 Hz
SS2	12.4 Hz	12.06 Hz	11.8 Hz	9.06 Hz	11.45 Hz
fore-aft 1	1.7 Hz	1.7 Hz	1.7 Hz	1.73 Hz	1.7 Hz
foreaft 2	11.9 Hz	9.7 Hz	11.8 Hz	9.5 Hz	11.3 Hz
fore-aft 3	-	21.5Hz	34.1 Hz	28.5 Hz	30.08 Hz

The first periods obtained from all the analysis show a good agreement with each other. This is due to the fact that including the rotor to the FEM does not have a significant effect on the first natural period. Most of the early studies also considered SDOF systems, which mainly means that they only considered the first mode of the structure in the seismic response. The second FA modes also show good agreement with the obtained results. The difference between the second FA period in both models draws some attention. The deviation can be due to the difference in the mass distribution. As for the second SS mode, the frequency obtained from the detailed model in this study is almost 30% less than the one obtained from the shake table test and UCSD model; however, it is worth mentioning that not many details with regards the analysis method of the blades is provided in previous studies. Based

on the publications from the series of shake table tests [3, 4], the natural frequencies obtained belong to the tower. It is believed that only the distribution of the mass is taken into account and not the stiffness of the blades, which can cause the differences between the second and higher modes in both directions. Also it should be mentioned that the distributed mass and stiffness over the blades in this study is not exactly as the real structure due to the lack of necessary details. The deviations between the results can also be caused by these uncertainties. Overall, the results of this study is convincing since the uncertainties can cause some minor deviations.

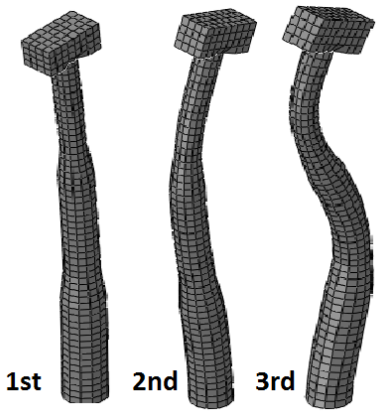

Figure 2.6. Fore-aft mode shapes for the lumped mass model.

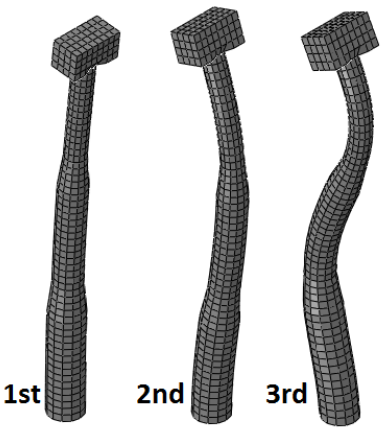

Figure 2.7. Side-to-side mode shapes for the lumped mass model.

2.4. Damping

The damping ratios for the first two modes of the wind turbine are reported amongst the UCSD results [4]. It is also mentioned that the modal damping ratio for the first modes can be considered as 1% [3] , and that for the higher modes the damping ratio is around 3%. Damping in the SS direction is slightly bigger than the FA direction. Table 2.3 specifies the exact values of damping ratio for each mode [4].

Table 2.3. Obtained modal damping ratios by Prowell et al., [4].

Mode	Modal damping ratio %
1st SIDE-SIDE	0.57
2nd SIDE-SIDE	0.84
1st FORE-AFT	1.6
2nd FORE-AFT	1.9

2.5. Modal Analysis and Validation of the Time-history Results

In this section, the time-history results obtained via modal analysis are evaluated in the context of the UCSD experiment. During the shake table tests, the ground motion is applied along the SS direction of the wind turbine, and the operating condition of the turbine is the parked state.

2.5.1. Earthquake Records

The ground motion applied is the Landers earthquake of June 28, 1992 [5]. Some selected specifications of the earthquake are presented in Table 2.4. Prowell et al., [1] scale the earthquake to 100%,150% and 200% in the shake-table tests and their numerical analyses. In the current analysis only the 100% (original record) is utilized. Figure 2.8 displays the ground motion acceleration. Figures 2.9 also displays the response spectra of the earthquake.

Table 2.4. Landers Earthquake specifications [5].

Parameter	Data
Name	Landers
Date	26th June, 1992
Country	USA
Station	CDMG 12149 Desert Hot Springs
Station Direction	DSP090 (east-west)
Falut Distance	23 km
V_s,30	345.40 m/s
Mw	7.28
Peak Ground Acceleration	0.154 g
Root-Mean-Squared acceleration	0.266 g
Arias Intensity	0.678 m/s
Relative Significant Duration	31.98 s

Landers earthquake is a desirable ground motion with regards to obtaining the seismic response of the 65kW wind turbine. The ground motion's characteristics are suitable for analyzing the wind turbine, since it can excite all the possible modes of the structure.

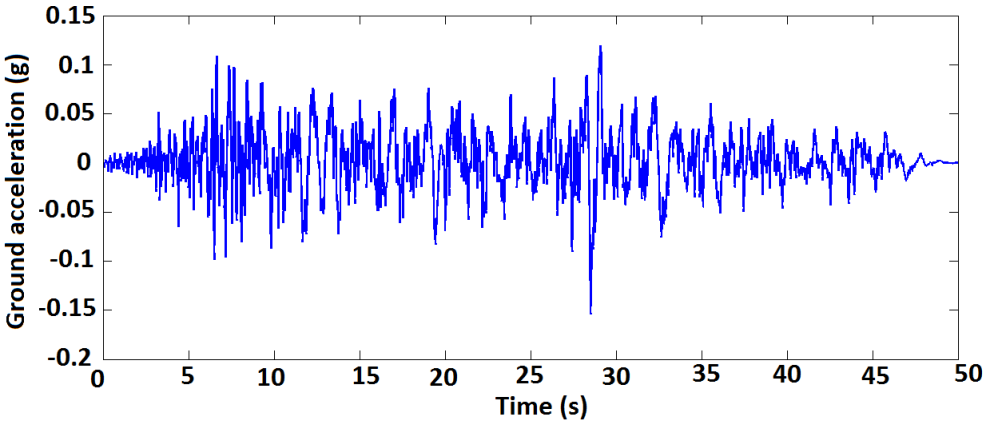

Figure 2.8. Landers earthquake ground acceleration time-history.

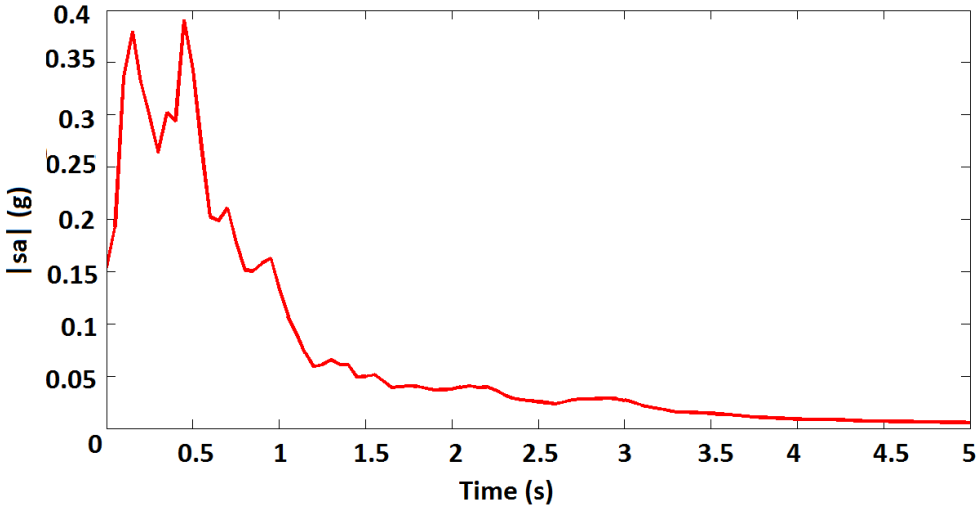

Figure 2.9. Landers earthquake response spectra.

It can be observed that Landers earthquake mostly affects those frequencies between 1-10 Hz. The wind turbine's first and second side-to-side modes are in this range (Section 2.3.2). On the other hand, these modes are not significantly affected by the existence of the blades. Therefore, the differences between the time history results of the lumped mass model and the detailed model subjected to the Landers earthquake is expected to be very low.

2.5.2. Modal Dynamic Analysis Results and Comparisons with the Shake-table Test

Peak accelerations at the top of the nacelle is a good factor to be evaluated for the investigation of the effects of an earthquake on a wind turbine [28]. During the shake table test, 3 sensors were installed on the wind turbine to record the accelerations. Figure 2.10 displays the Nordtank 65 kW wind turbine tested in the UCSD experiments along with the location of the sensors.

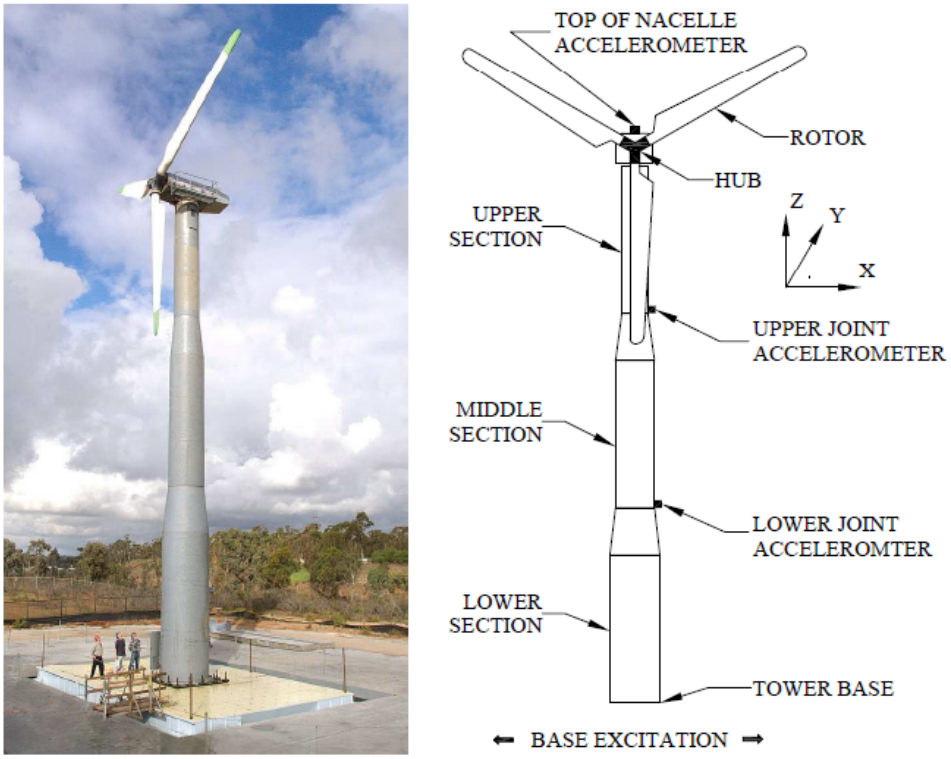

Figure 2.10. Nordtank 65 kW wind turbine: sensor locations [1].

Acceleration time-history results were obtained in this study for the detailed model. Figure 2.12 displays the time history outputs obtained via modal analysis of the numerical model. Figure 2.11 shows the results from the shake table test. The results show a good agreement, the peak response obtained in the current study is bigger than the ones obtained from the numerical model in [3] and the ones from the shake table test (by around 10%) which can be due to some uncertainties regarding the properties of the structure and some other factors such as:

(i) The differences in the input : The excitation produced by the shake table test can not be exactly as the one obtained from PEER [5].

(ii) Due to the characteristics of Landers earthquake, the second bending mode also has some effect in the response. According to the results obtained by [3], the second bending mode is higher than the one obtained in the current study (by

around 30%) which can also be the reason why the time history results are not exactly the same.

(iii) It is also important to mention that the blade models are not precise, and the distribution of rotor's mass between the hub and blades was not specified by Prowell et al., [3], which can also be another reason for the differences.

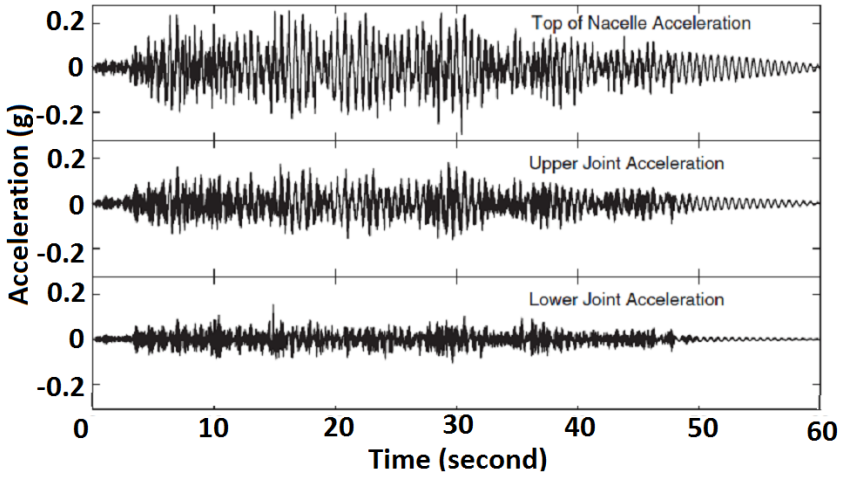

Figure 2.11. Acceleration time-history recorded during the shake-table test [3].

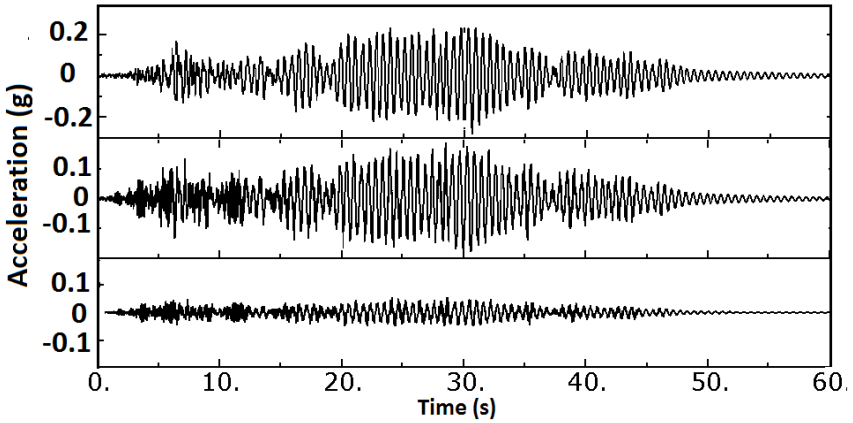

Figure 2.12. Acceleration time-history results obtained in the current study.

2.6. A Basic Study on the Importance of Adding the Blades to the Finite Element Model

In this chapter, a series of analyses are discussed with the aim of comparing the differences between the time history results of the two numerical models. The first model considers the blade's mass as a lumped mass on the top. The second model is a detailed model including the blades.

2.6.1. Earthquake Records

Three different ground motions are selected to be used in the analyses based on the experiment: Landers Earthquake, Imperial Valley and Palm Springs. All three earthquakes are Los Angeles, California earthquakes, and they are chosen as they are believed to excite the modes of the structure well [4] and their characteristics are similar to those ground motions observed in Turkey. Table 2.5 displays various information regarding these records. The response spectra of each component of each of these earthquakes are shown in APPENDIX B. These spectra were obtained by the code.

Table 2.5. Information about the four chosen earthquake records.

Earthquake	Station	Fault Distance	Mw	PGA
Landers 26th June 1992	Desert Hot Springs	21.78 km	7.28	0.154 g
Imperial Valley 15th October 1979	El Centro Array #5	1.76 km	6.53	0.45 g
North Palm Springs 8th July 1986	5070 Palm Springs	4.04 km	6.06	0.59 g

2.6.2. Nonlinear Time-history Analysis with Direct Integration Method

In order to capture the failure modes of the wind turbine, series of nonlinear time history analysis are conducted with different ground motions. However, prior to such analyses, it is important to make sure that the direct integration method yields reliable results for the model. Unlike other softwares commonly used in civil engineering that are designed to run seismic analysis, ground input is only defined in ABAQUS for linear

dynamic analysis where the equation of motion is solved with modal superposition [29]. To make sure that it is possible to capture the seismic response of a structure through the direct integration method, a comparison between the time history results obtained via each method is made. Prior to such analyses, careful considerations needed to be made regarding the induced damping in direct integration method.

2.6.3. Damping

The general form of the equation of motion may be expressed as

$$\Big[M\Big]\Big\{\ddot{u}(t)\Big\} + \Big[C\Big]\Big\{\dot{u}(t)\Big\} + \Big[K\Big]\Big\{u(t)\Big\} = \Big[F(t)\Big] \tag{2.2}$$

where $\Big[M\Big]$, $\Big[C\Big]$ and $\Big[K\Big]$ are the mass, damping and stiffness matrices, respectively; and the forcing function matrix $\Big[F(t)\Big]$ on the right hand side is a function of support motions. The displacement vector $\Big\{u(t)\Big\}$ may be defined either as the absolute response or the relative (to the ground) response, depending on how the problem is formulated (the dots over the response denote time differentiation). While solving the equation of motion in 2.2, the damping matrix is difficult to construct, and there are several ways for defining the damping matrix. A well known approach is using the Rayleigh damping, which is a linear combination of the mass matrix and the stiffness matrix using two coefficients α and β:

$$[C] = \alpha\,[M] + \beta\,[K] \tag{2.3}$$

The modal damping ratio,ζ_i, of the ith mode can then be expressed in terms of the coefficients α and β, and the circular frequency, ω_i of that mode, as follows:

$$\zeta_i = \frac{\alpha}{2\omega_i} + \frac{\beta\omega_i}{2} \tag{2.4}$$

The above equation can be solved to obtain the desired damping ratios in two modes by solving for the coefficients α and β to achieve the specified values. For the subsequent

analyses herein, the damping value is specified for the first and fifth modes. However, it should be noted that this may result in overestimated damping for the higher modes [31].

Considering this issue, a comparison was made between the modal dynamic time history results and the direct integration method. The results were in a good agreement with each other. Therefore, the chosen damping ratios are deemed acceptable. For the sake of argument, it needs to be said that although the results are satisfactory, one reason can be that the first modes in the turbine are the most dominant, such that the expected higher damping in higher modes do not significantly effect the results.

2.6.4. The Method of Subjecting the Structure to Ground Motion

In implicit integration, the ground motion is applied as a boundary condition. A reference point is fixed on the ground and all the base nodes of the tower are constrained to move with that point. The reference point is made to move as prescribed by the ground motion and the response of the structure is obtained. The displacement output is the total displacement. The relative displacement needs to be calculated separately.

After the proper adjustments and calibrations are made, the time history results obtained from the modal analysis are compared with those obtained via the direct integration method. The deviation between the results remains less than 0.1 %; therefore, the adjustments are concluded to function correctly.

2.6.5. Simplified FEM vs. Detailed FEM

After calibrating the direct integration method, in this section, the effect of a detailed model will be investigated. Two different models will be compared. The first model considers the rotor as a lumped mass on the top, however the nacelle stays as it is.The second model is a detailed model of the whole structure including allthe structural elements which may affect the seismic response. The response of thedetailed

model in SS direction and FA direction will be compared too. The top acceleration is the main factor which will be compared among these models.

(i) Landers Earthquake:

The differences between the seismic responses of the two models subjected to the Landers record is significant. The peak acceleration in the detailed model is about 28% bigger than the value obtained via the model without the blades. This can be due to the characteristic of the earthquake. Considering the response spectra of the ground motion in Figure 2.9, the second bending modes are also excited, as for the detailed model the frequency is 30% less that the simplified model. Therefore, the difference between the time-history results can be caused due to this phenomenon. There is also a shift in the frequencies which displays the differences between frequencies of the two models. The difference is observed in both the FA direction and the SS direction. Figures 2.14 and 2.15 display the difference between the time-history result of top acceleration obtained via the two FEM models in the SS and the FA direction respectively. Figure 2.13 displays each mode's mass contribution to the response.

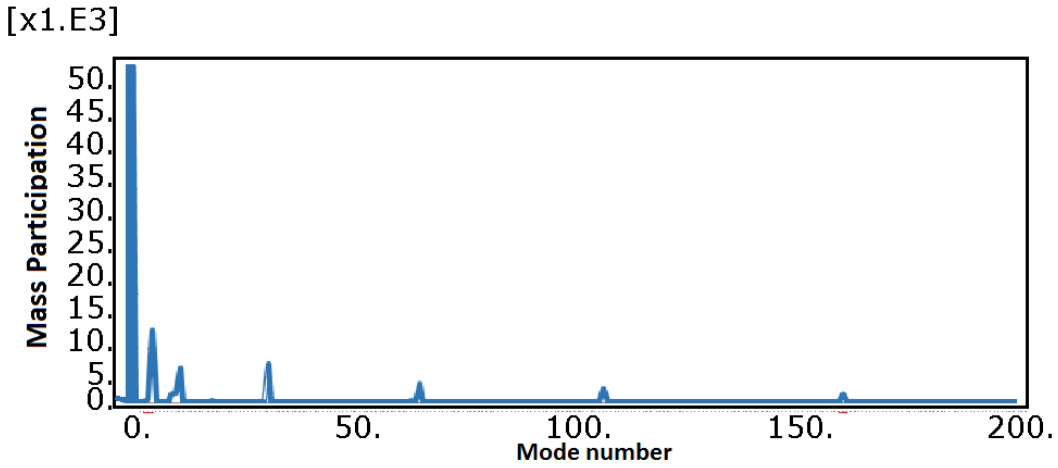

Figure 2.13. Mass contribution of the detailed model between the modes.

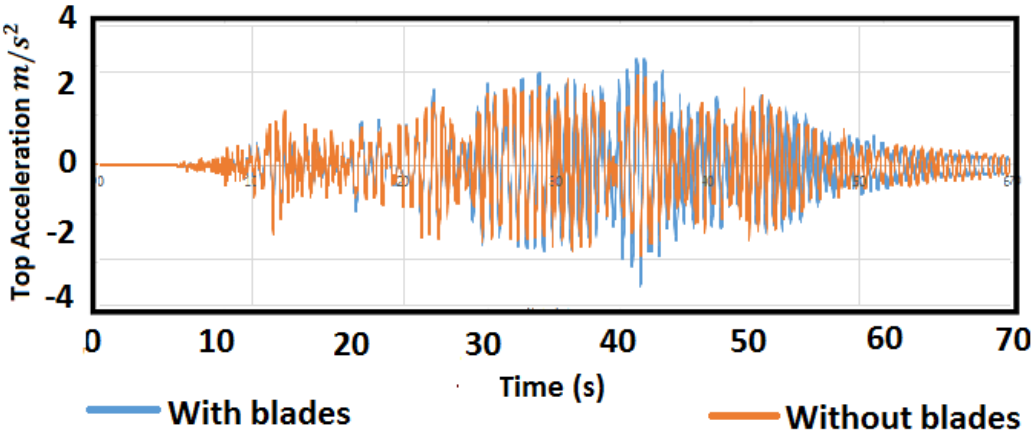

Figure 2.14. With blades vs. without blades, SS direction, Landers ground motion.

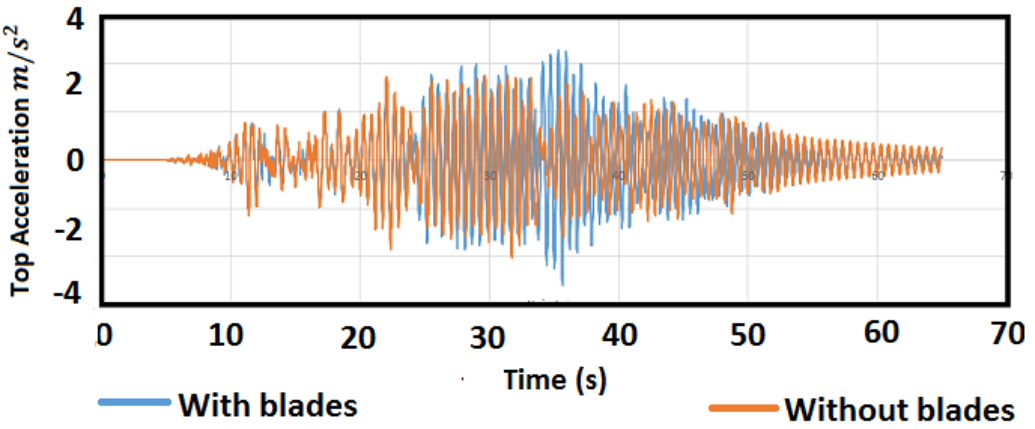

Figure 2.15. With blades vs. without blades, FA direction, Landers ground motion.

(ii) Imperial Valley Earthquake:

Imperial Valley record does not excite the second mode as severely as the first mode, therefore, the difference between the lumped mass model and the detailed model is not very significant. This ground motion mainly excites the first bending mode; therefore, for the 65 kW wind turbine, it does not make a difference if the model is detailed or lumped. Besides, the response of the structure subjected to this ground motion in the SS and the FA directions are almost the same due to the same reason. Figure 2.16 displays the comparison between the two FEM models in the SS direction.

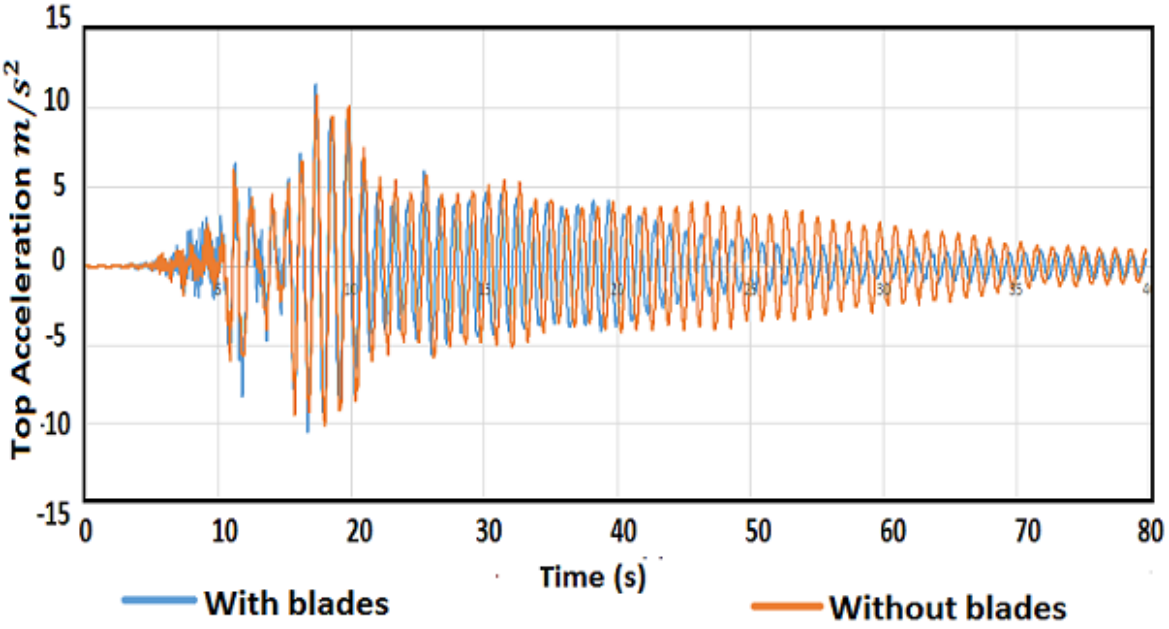

Figure 2.16. With blades vs. without blades, SS direction, Imperial Valley ground motion.

(iii) N.Palm Springs Earthquake:

The differences between the peak response of Palm Springs Earthquake is not significant as well. The response spectra of the earthquake also displays that the dominant mode is the first mode, and higher modes do not have a significant effect on the seismic response. Therefore, the difference between the two FEMs are also not significant. There is also a shift in frequencies which can be observed between the models which explains the differences between the natural frequency of the two model. There is a difference between the response magnitude observed in the free vibration part. The difference is due to damping. The main focus in this part was the difference between the peak acceleration in each model. in order to match the results perfectly, better considerations need to be made for obtaining good values for Reighley damping coefficients. The lumped mass model experiences less damping than the detailed model. Although, for the 65 kW wind turbine, a detailed model seems to be unnecessary in most cases, for taller turbines, their higher modes also fall in to the frequency range of the ground motion, and adding the blade to the finite element model will be more critical.

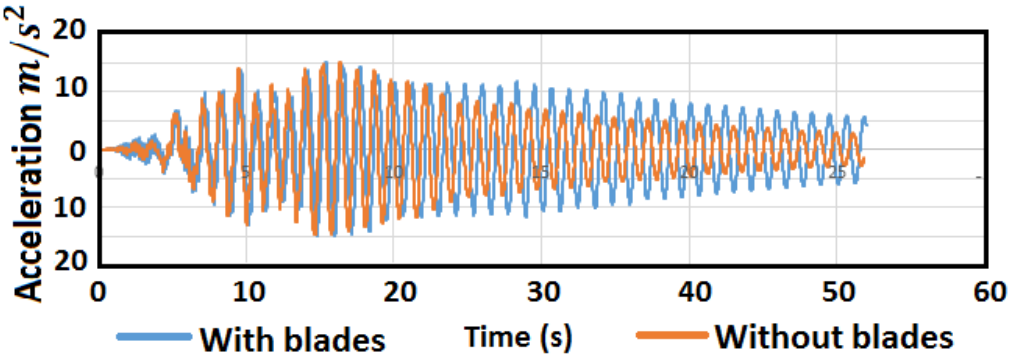

Figure 2.17. With blades Vs. without blades, SS direction, Palm Springs.

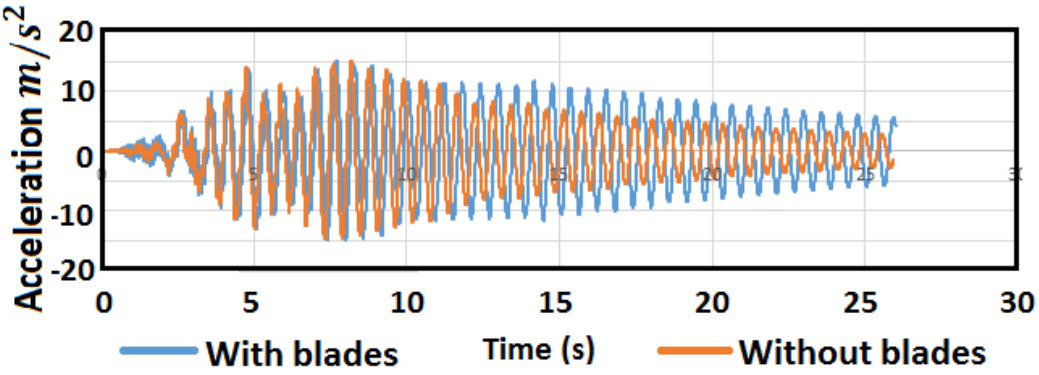

Figure 2.18. With blades Vs. without blades, FA direction, Palm Springs.

2.6.6. Nonlinear Time-history Analysis

The 65 kW wind turbine is pushed to a level so that it would show some non-linearity. The aim is to observe if it is possible to capture the failure modes and shell buckling. The Landers record is magnified by 7 when the first bucking happened. As it should be expected, the first buckling happens around the lower joint [1]. Figure 2.19 displays the buckling in the tower. The induced PGA is 0.9g; the peak acceleration observed is 30 m/s^2 on top of the nacelle, which is almost 10 times more than the measured acceleration in the shake table test. It is important to mention that this PGA is not the ultimate PGA for failure, it is believed that different earthquakes with

undesirable characters may cause failure with a smaller PGA. However, the difference will not be crucial. In general the odds that the 65 kW wind turbine's tower will fail due to seismic excitation seems very low.

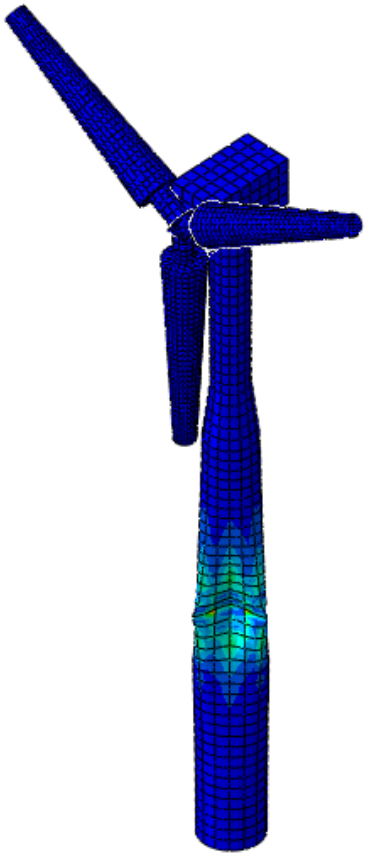

Figure 2.19. Buckling of the 65kW wind turbine tower.

3. SEISMIC ANALYSIS OF THE BÜRES 900 KW WIND TURBINE

After achieving fairly reasonable results from the numerical analysis of the 65 kW wind turbine, and thereby gaining knowledge and assuring that the numerical model is capable of capturing the seismic response, modeling a modern wind turbine is perused. Boğaziçi University has recently installed a modern wind turbine in its Sarıtepe campus. The turbine is capable of supplying the whole electricity demand of the campus. In this chapter, seismic response of BÜRES wind turbine is investigated. The structure has an emergency shut down system which is sensitive to the level of vibration. In cases such as a wind speed higher that the cut-out speed and a seismic excitation, the break will stop the rotation of the rotor immediately. Therefore, in this thesis the seismic response of the wind turbine will be obtained in its parked condition. Although, it is better to consider the moment caused by the emergency shut down, in this thesis in order to simplify the analysis, the moment was not considered.

3.1. Dimensions and Material Properties of the BÜRES 900 kW Wind Turbine

The BÜRES wind turbine has a hub height of 55 m. The rotor diameter is 44 m. The tower is made of cold formed steel with an elasticity modulus of 200 MPa. Its weight is 534 kN. Its cross section diameter at the base is 3.3 m, and at the top it is 1.6 m. Figures 3.2 and 3.1 display the shape and size of the structure. Table 3.1 shows the general specifications of the wind turbine.

The total weight of the nacelle plus rotor is 326 kN and each blades' wight is approximately 1800 kN. The blade's cross section data is available. Figure 3.3 displays the dimension of the blade. Although all the specifications (e.g. its wall thickness) of the blade is not available, the first natural frequency of the blade is measured on site to be about 0.8 seconds. The stiffness and the mass of the blade are calibrated

based on the available data. Knowing the mass and the project surface of the blade, it is possible to estimate a constant thickness for the whole blade. Based on that, the elasticity modulus of the blade is calibrated in order to obtain the target natural period. By reaching the right period for the blade, it is possible to obtain an acceptable detailed model of the wind turbine with a reasonable distribution of mass and stiffness. The tower's density is also user-defined based on its mass and volume for the accuracy of the analysis. The wind turbine tower's thickness varies along its hight. Two models are obtained in order to observe the influence of the design on the seismic response of the structure on its failure. The first model has a constant thickness of 22 mm and the second model is consistent with the exact design on the tower. Figure 3.1 displays the details of the tower height and thickness. The opening of the tower was not modeled in this thesis.

Table 3.1. 900 kW wind turbine's technical specifications.

Rated Power	99kW
Rotor diameter	44m
Hub height	55m
Rotor type	Upwind rotor with active pitch control
Rotational direction	Clockwise
Swept area	1.521 m^2
Blade material	GPR (epoxy resin) Built-in lightning protection
Rotational speed	Variable 16-34.5 rmp
Hub	Rigid
Main bearing	Twin tapered roller bearing
Brake system	-3 independent pitch control system with emergency power supply -Rotor break -Rotor Lock
Cut-out wind speed	28-34 m/s with storm control

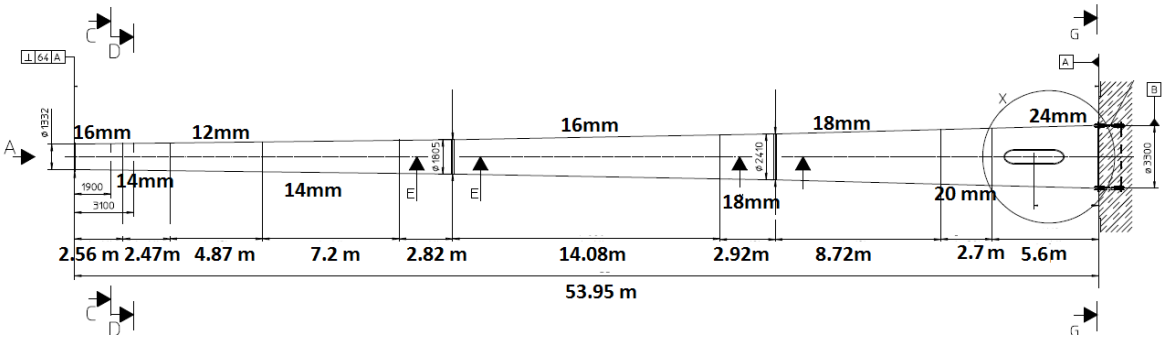

Figure 3.1. 900 kW wind turbine tower and its dimensions.

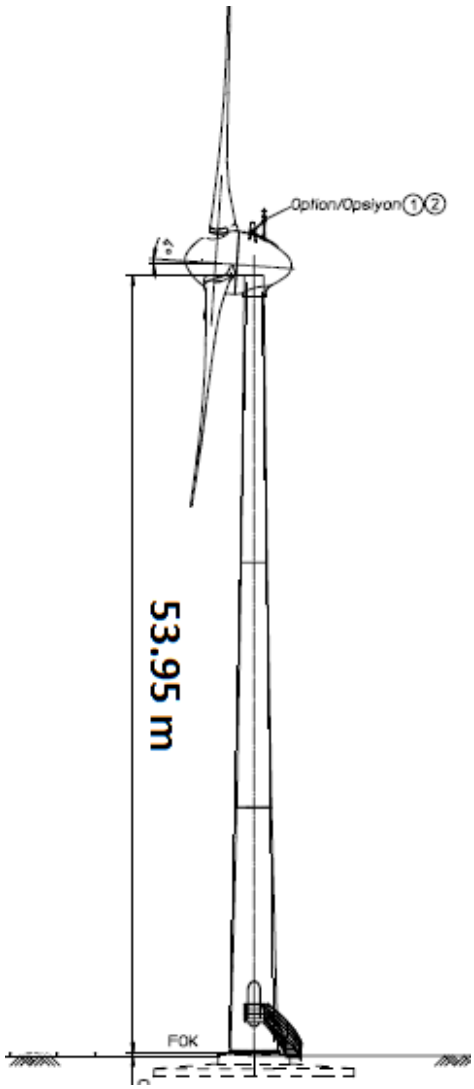

Figure 3.2. 900 kW wind turbine figure.

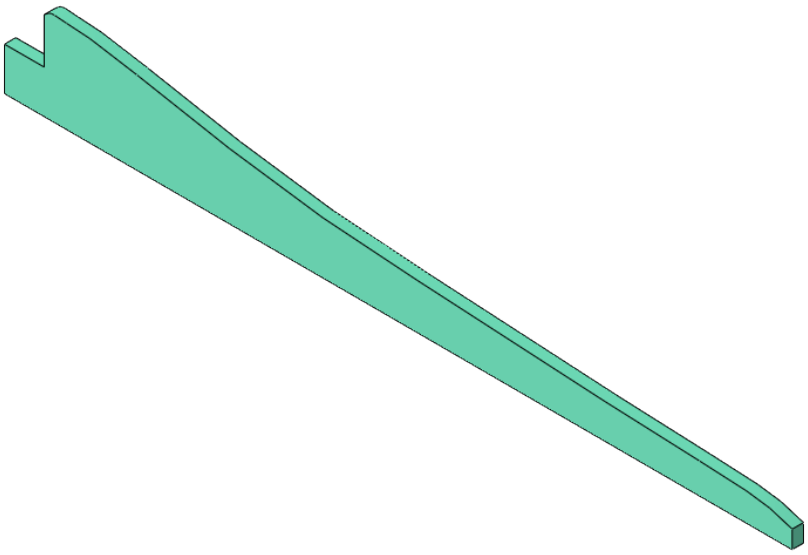

Figure 3.3. Schematic sketch of the cross section of the blade.

3.2. Finite Element Model and Natural Frequencies

Knowing the material properties and the dimensions of the structure, a finite element model is constructed. Figure 3.4 displays the FEM obtained in ABAQUS. The tower was modeled using 8 noded shell elements. The blades are also modeled as shell elements. The nacelle is modeled with rigid solid elements. The connection between the blades and the hub is rigid.

The natural frequencies of the structure are extracted. The first period is around 2 seconds in both the SS and the FA directions. Figures 3.5 and 3.6 show the first three mode shapes of the BÜRES turbine in both directions. It can be seen that higher modes are more affected by the blades and coupling can be observed. The first frequency of the 900 kW turbine is almost 1/4th of the 65 kW wind turbine. This means that an earthquake with a characteristic similar to Imperial Valley (1979) might even be less critical for this turbine, considering the first bending modes. The results of the analysis related to this issue will be discussed shortly.

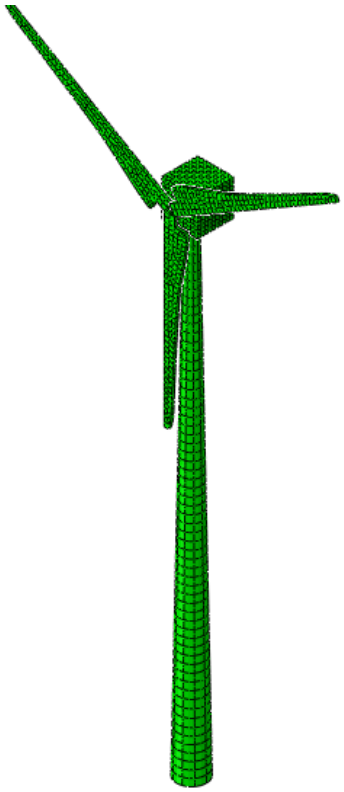

Figure 3.4. Finite element model of BURES wind turbine.

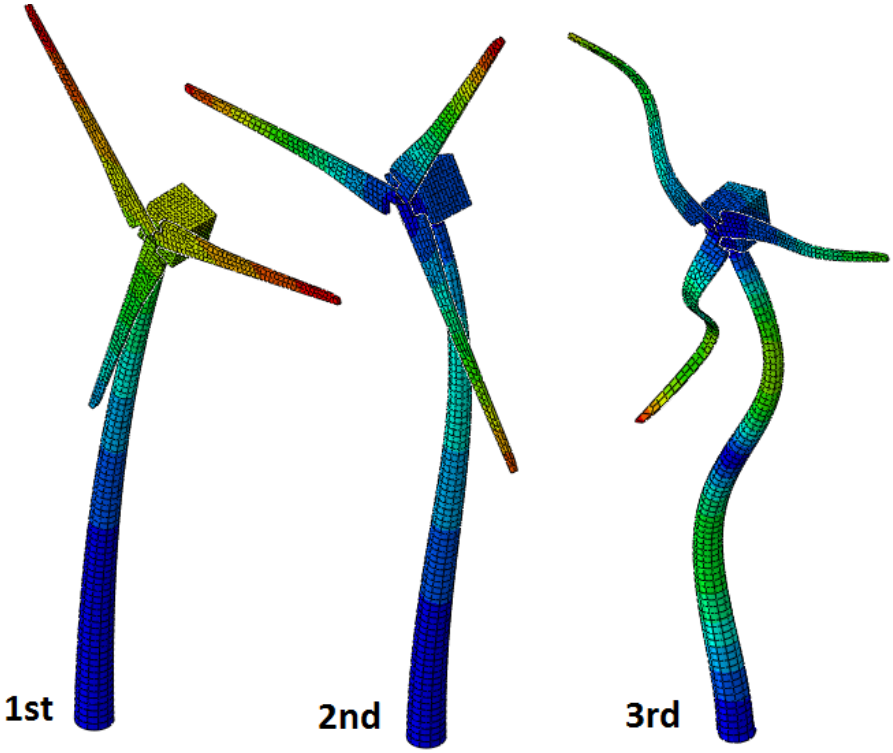

Figure 3.5. SS mode shapes.

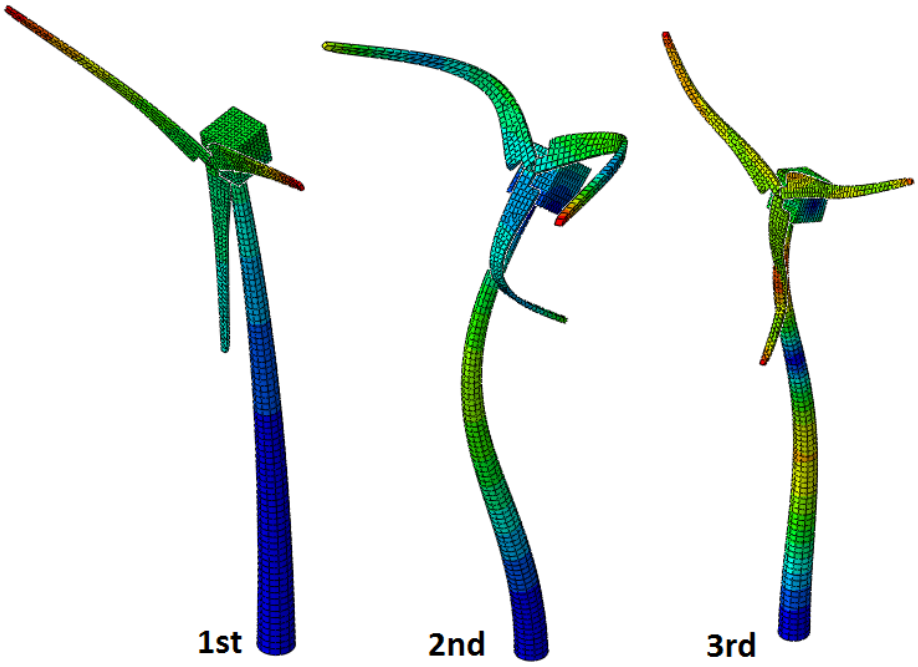

Figure 3.6. FA mode shapes.

3.3. Damping

The same method as the Nordtank wind turbine is used for the application of damping in direct integration analysis. The damping of the wind turbines are generally around 1% [1] while parked . Initially a modal analysis is conducted similar to the 65 kW wind turbine. Afterwards, α and β are calculated based on the first and the fifth modes of the structure. Their periods are 2 and 0.0125 seconds, respectively. The calculated α and β are given as input for Rayleigh damping to dynamic implicit analysis. In order to make sure that the given values are consistent with the actual damping of the structure, a simple analysis is conducted in which an initial displacement of 50 cm is induced to the top of the nacelle in both cases and free vibration results are compared. There is a minor frequency difference between the two methods, and this difference becomes more obvious as the tower freely vibrates for 30 sec. The response amplitudes, however, are in consistent with each other. therefore, the chosen coefficients are satisfactory.

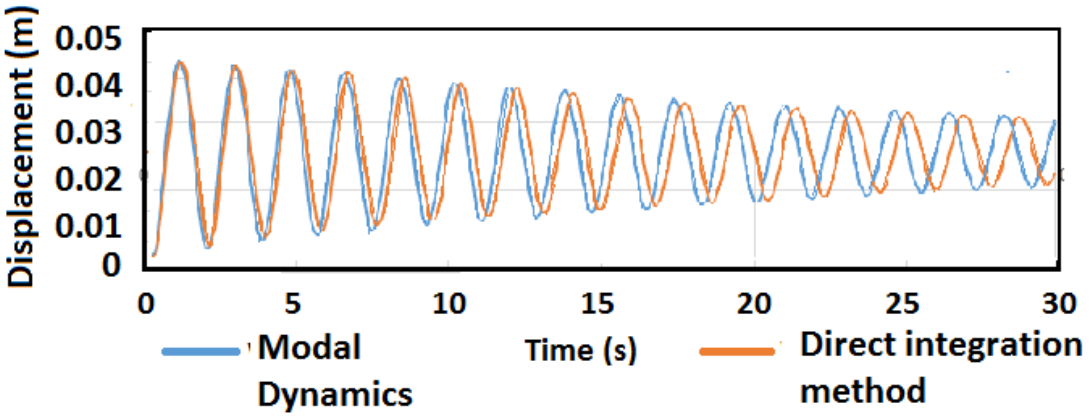

Figure 3.7. Comparison between the free vibration of modal dynamics and direct integration method.

3.4. Ground Motion Inputs

Table 3.2. Specifications of the ground motions.

Earthquake	Station	Mw	PGA
Landers 06.26.1992	Desert Hot Springs	7.28	0.154 g
Imperial Valley 10.15.1979	El Centro Array #5	6.53	0.45 g
Imperial Valley 05.19.1940	El Centro Array#9	6.95	0.3 g

The ground motions chosen for this analysis are summarized in Table 3.2. These are three chosen earthquakes from the LA earthquake suite which is made up of 10 recorded earthquakes (20 records for the orthogonal components of the earthquake), compiled and scaled by Somerville et al., [32]. Figure 3.8 shows the response spectra of the chosen earthquakes and their mean spectrum in comparison with the Turkish design spectrum. We obtain an average close to the 1g design spectrum by magnifying all of these motions to 300% of their original records. The structure is be analyzed by these three magnified ground motions. Figure 3.9 displays the response spectra and mean value of the magnified ground motion inputs versus the design spectrum. However, it should be noticed that based on site conditions the design spectrum will be multiplied by an amplification factor. Therefore, amplifying the chosen ground

motions puts them considerably above the expected hazard level. the North Palm Springs earthquake record leads to spectral values way above acceptable levels, and therefore the seismic response of the structure subjected to this earthquake was not considered in this chapter.

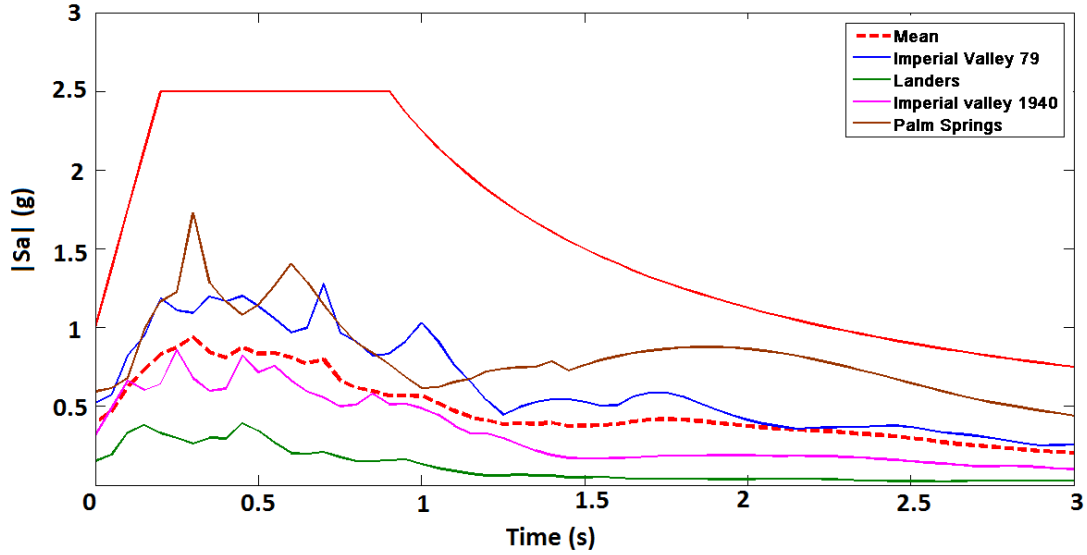

Figure 3.8. Response spectra of selected ground motions vs. the design spectrum.

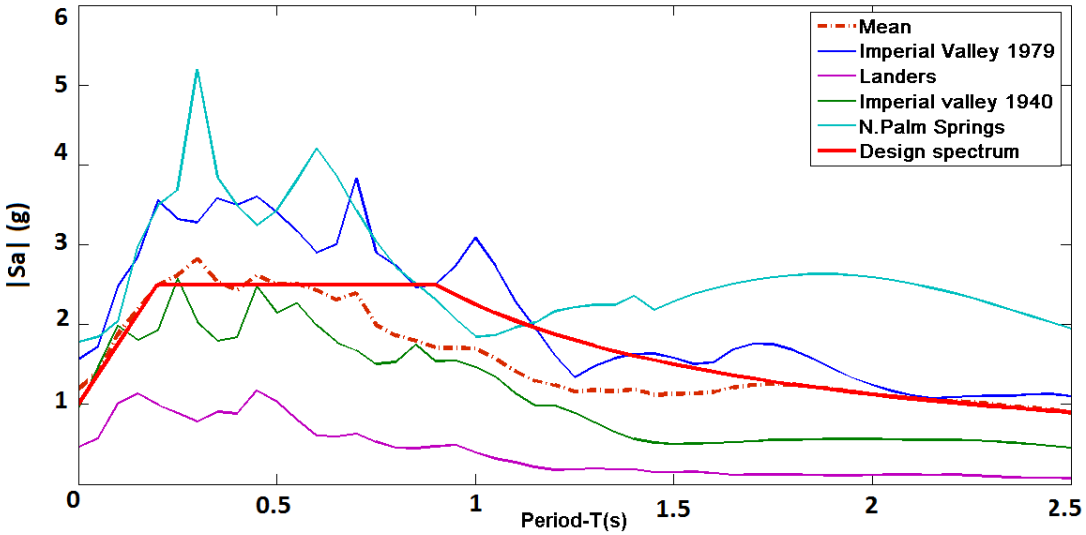

Figure 3.9. Response spectra of the amplified (scaled to 300%) ground motions vs. the design spectrum.

Based on the earthquake characteristics and their mean, it is believed that the first mode will be contributing the most to the response since it withholds a great portion of the mass. Figure 3.11 displays the mass distributions between each mode. The second mode will also play an effective role in the seismic response of the structure, since it coincides with the maximum value of the mean response spectrum. Other modes will also participate, but their participation will not be as significant as the first two modes. The first three periods are marked on the mean response spectra (Figure 3.10). It is also worth mentioning that considering the natural periods of the structure, the mean spectra can be a representative of the design spectrum of the site. Although the mean spectra is a bit below the design spectrum in some areas of the plot, the wind turbine's natural frequencies do not fall in that interval.

From the mean spectrum, it can be concluded that the first three modes of the structure will get excited by the selected ground motions. Besides, it is worth mentioning that the second mode is the most critical one, considering the spectral acceleration.

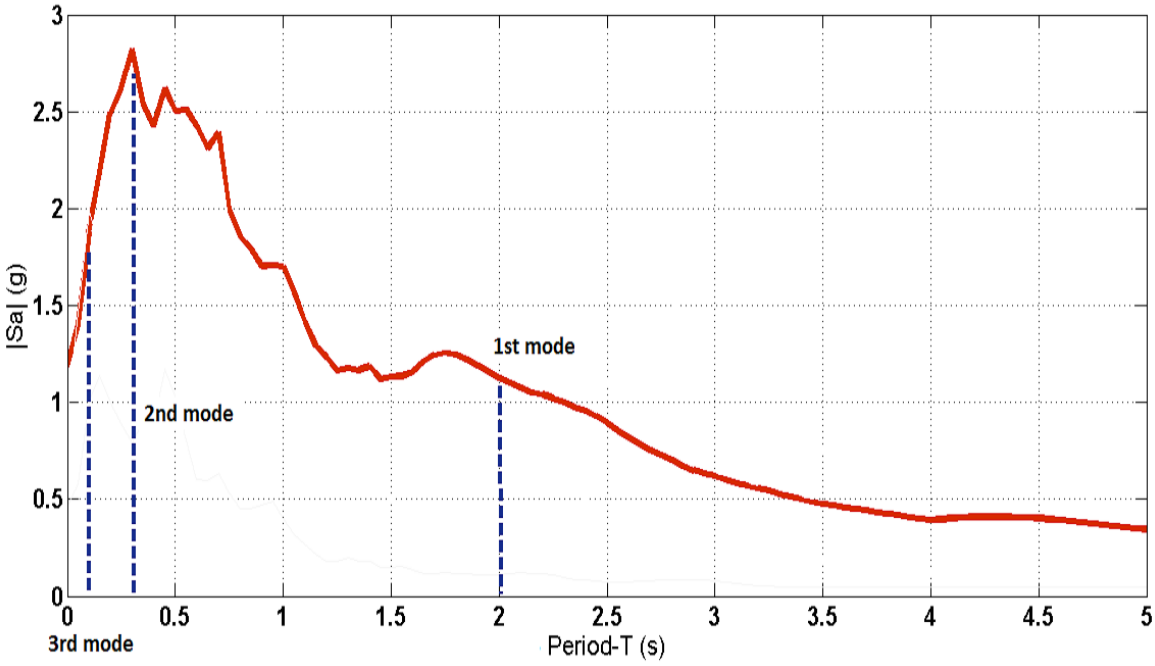

Figure 3.10. Mean spectrum.

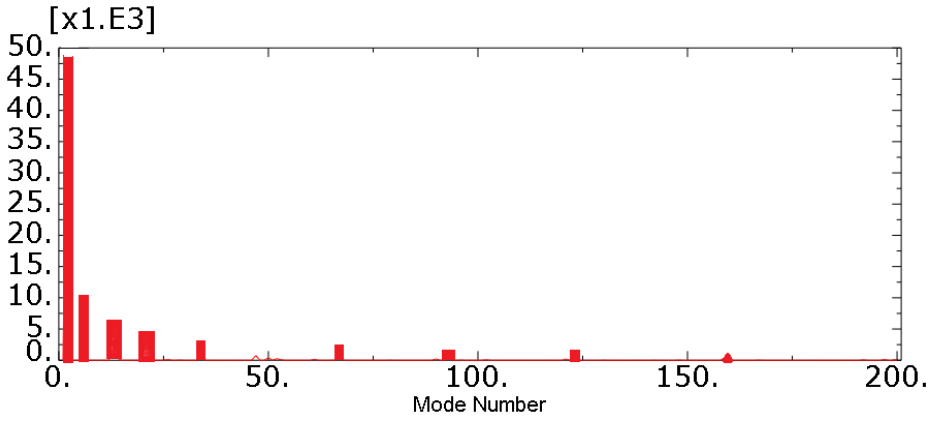

Figure 3.11. Mass contributions of the modes in the SS direction.

3.5. Nonlinear Time-history Analysis

From all the factors that need to be observed carefully with regards to the seismic response of structures, there are some that can be representative of the failure state of the structure. For wind turbines, keeping track of the top acceleration, the top displacement and the base moment can be a good approach for evaluating their seismic response. In special cases such as BÜRES and Nordtank wind turbines, the areas along the cross section of the tower where the cross section's area changes are also critical.

3.5.1. Comparison Between the Two Tower Sections

Initially in this part the importance of a detailed model of the tower is discussed and its influence on the response of the whole structure is investigated. As it has been mentioned, two different models are analyzed. In the first model, the tower has a constant thickness of 20 mm. In the second one, the tower's thickness changes through its height (Figure 3.1).

The failure modes observed between the models are different. As it has been predicted, the thickness changes through the height increases the chances of buckling of the tower. Local buckling was observed in more than one location on the tower but mostly around 40 m from the ground where the thickness decreases from 16 mm to

14 mm and also at the location where it changes from 14 mm to 12 mm. As for the model with the constant thickness, the failure observed occurs only at the base. It is also important to mention that the thickness of the original tower at the base is 24 mm, which is 25% more than the thickness in the second model. This can explain why inelastic displacements are not observed at the base of the detailed model. Figure 3.12 displays the different failure modes of the tower in each of these structures under the amplified Landers record. The ground motion was multiplied by 5 in this case.

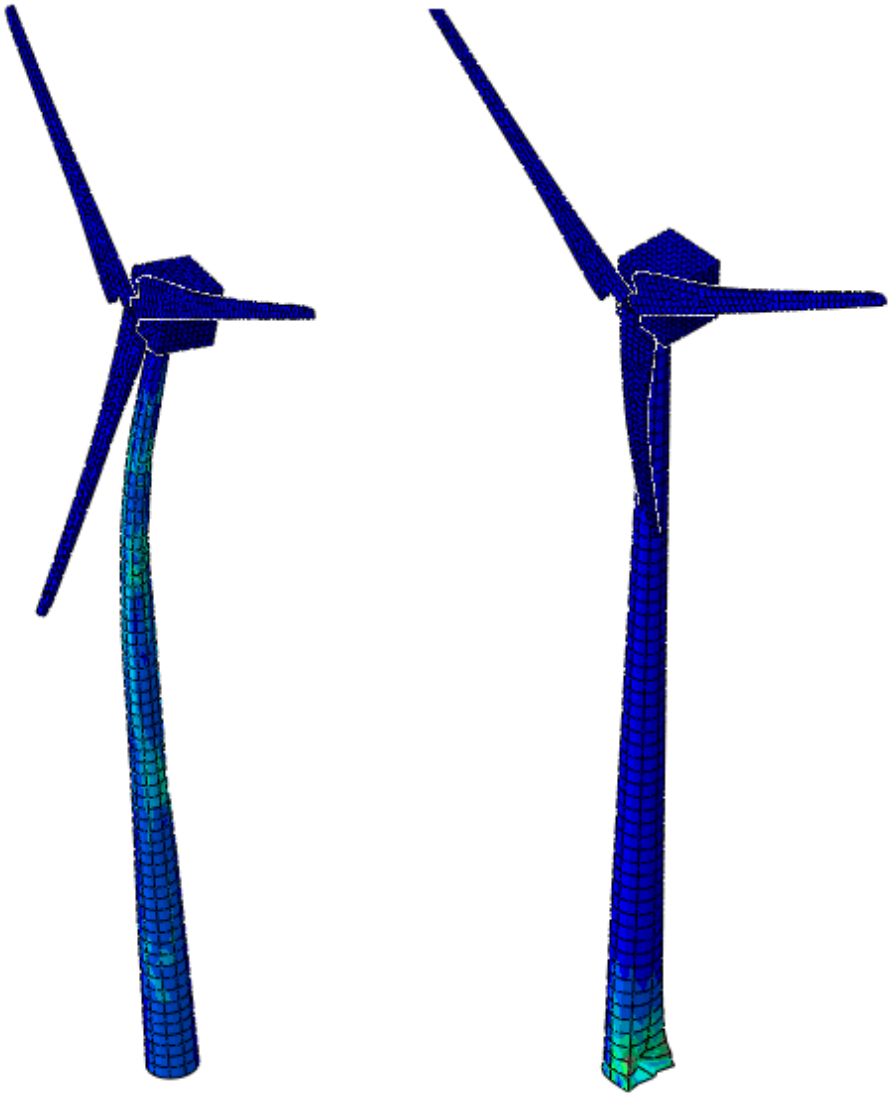

Figure 3.12. Failure modes.

3.6. Time-history Results of the Four Chosen Earthquakes

3.6.1. Time-history Results of Landers Earthquake

The wind turbine is subjected to the three components of the Landers record, each magnified by 3. The earthquake's PGA is 0.15g, which means that the input had a PGA of 0.45g. There is no failure observed due to this ground motion, which is rational since the spectra of the earthquake falls way below the design spectrum. The wind turbines are normally subjected to a significant level of vibration due to their operational purpose. It seems that the probability of failure of the wind turbine structure subjected to any level of earthquake below this is very low. Top displacement time-history results of the BÜRES wind turbine subjected to the Landers record are displayed in Figure 3.13. The rest of the time-history results are in APPENDIX A. The maximum displacement on top of the nacelle was observed to be around 1 m. The maximum base moment is approximately 70000 kN-m with respect to x axis .

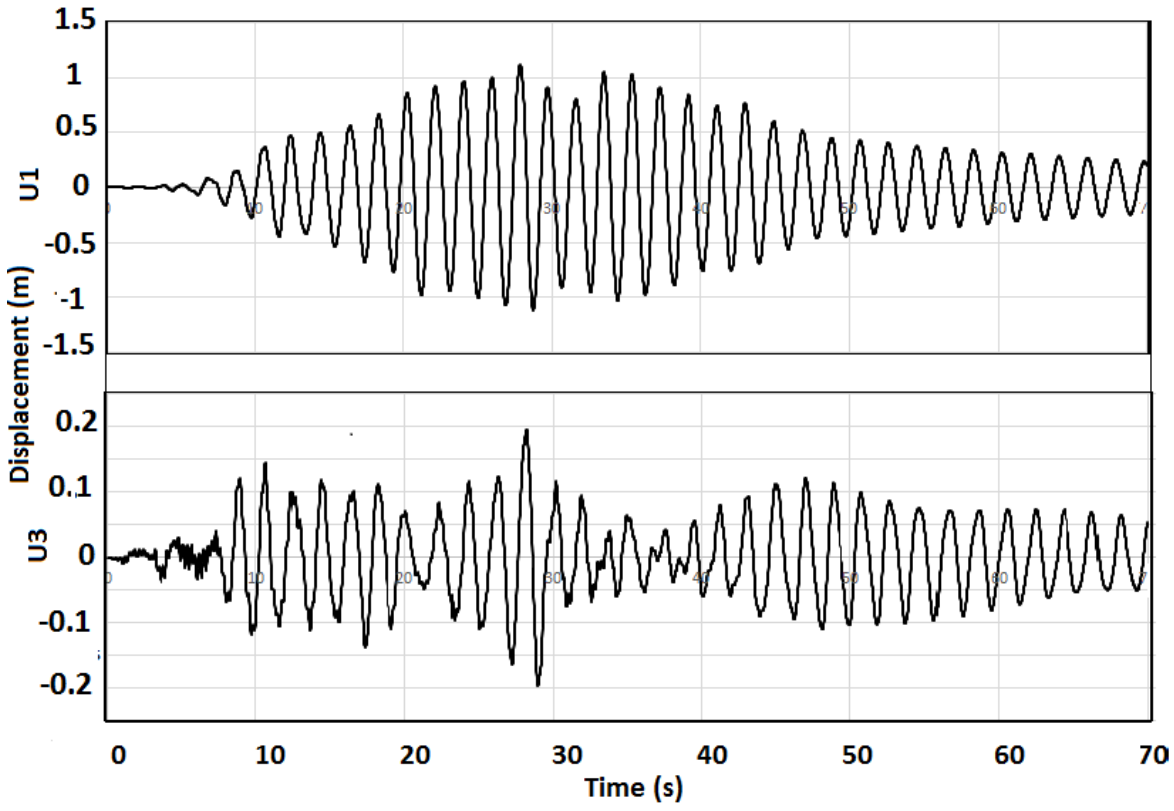

Figure 3.13. Top displacement in the horizontal x and z directions.

3.6.2. Time-history Results of Imperial Valley 1940 Earthquake

The second seismic excitation considered is the Imperial Valley 1940 record. The PGA of this earthquake is 0.3g and the ground accelerations are magnified by 3. Some inelastic behavior is observed on the tower, as expected. Buckling failure occurs at the height of 45 m where the thickness of the tower changes from 14 mm to 12 mm. Top displacement time-history results of the earthquake are shown in Figures 3.14 and 3.15. The rest of the time history results are plotted in APPENDIX A.

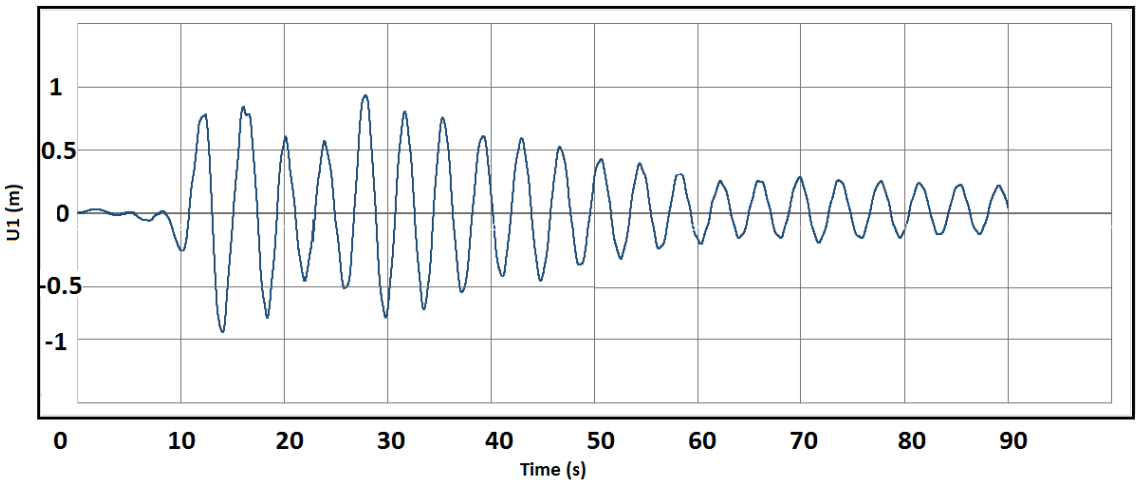

Figure 3.14. Top displacement in the horizontal x direction due to the amplified Imperial Valley 1940 record.

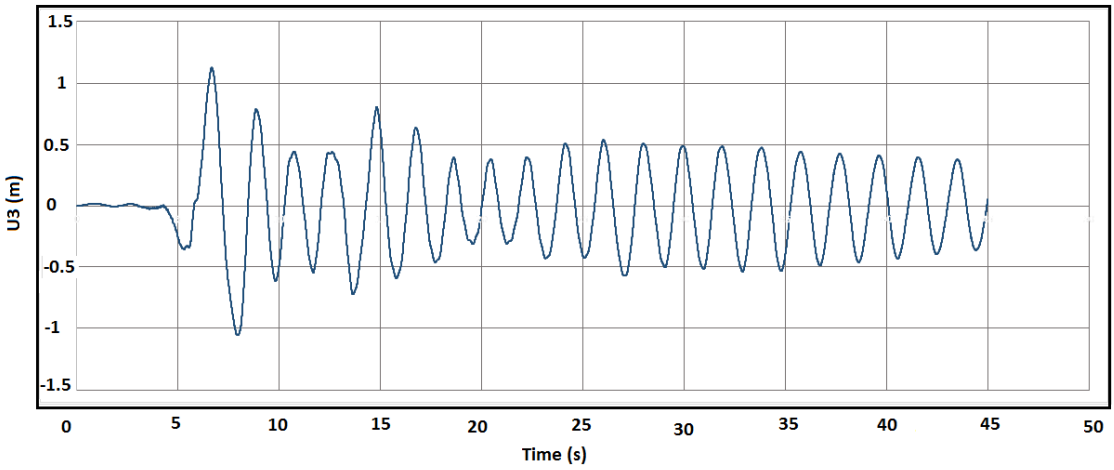

Figure 3.15. Top displacement in the horizontal z direction due to the amplified Imperial Valley 1940 record.

3.6.3. Time-history Results of Imperial Valley 1979 Earthquake

The Imperial Valley 1979 record magnified by 3 is even a more severe earthquake with a peak ground acceleration of 1.5g. This ground motion is somewhat unrealistic. Its response spectra falls above the design spectrum. The tower suffers more inelastic deformation around the areas where thickness changes, both around 35 m and 45 m along the height. Top displacement time-history results of the earthquake are shown in Figures 3.16 and 3.17. The rest of the time history results are plotted in APPENDIX A.

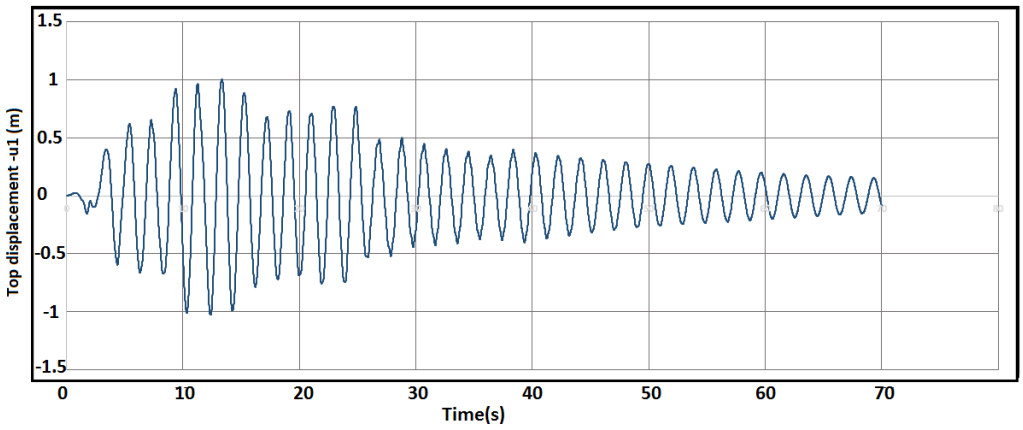

Figure 3.16. Top displacement in the horizontal x direction doe to the amplified Imperial Valley 1979 record.

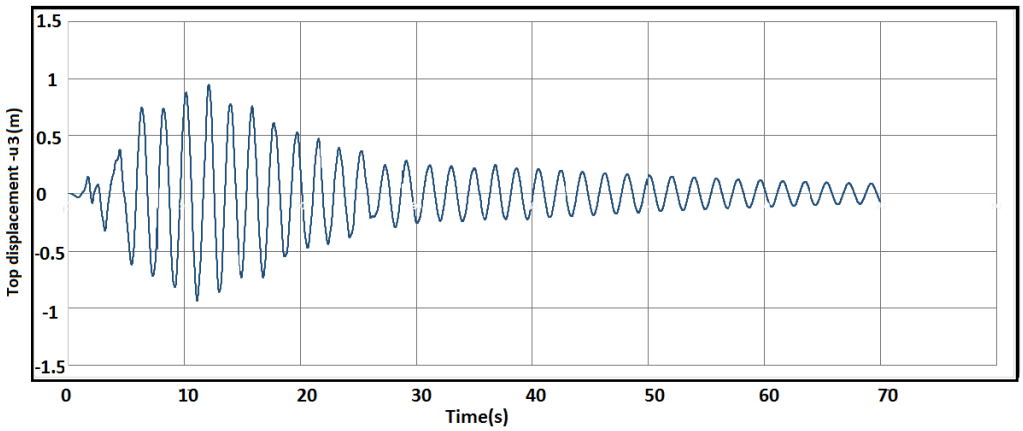

Figure 3.17. Top displacement in the horizontal z direction due to the amplified Imperial Valley 1979 record.

3.6.4. Comparison between the Peak Results and Demand

Table 3.3 displays the maximum base shear and base moment caused by each ground motion. Although these values were obtained with highly amplified ground motions, they could still be indicative of the importance of seismic loads in those areas where large seismic excitations are expected.

Table 3.3. Comparisons between the base shear and the base moment for amplified ground motion records.

Ground Motion	Fx KN	Fy KN	Fz KN	Mx KN.m	My KN.m	Mz KN.m
Landers EQ	400	600	400	7000	400	25000
Imperial Valley 1979	1250	3000	1100	30000	900	30000
Imperial Valley 1940	500	1200	800	25000	770	27000

4. CONCLUSIONS AND FUTURE WORK

4.1. Conclusions

(i) A detailed finite element model of two wind turbines were obtained. It was observed that adding the blades to FEM can result in a significantly different seismic behavior of the structure. The coupling between the blades and the tower affects the higher modes. For modern wind turbines higher modes also have a noticeable participation in the seismic response of the structure. Therefore, a detailed model is necessary. It was also observed that even for the shorter wind turbines subjected to an earthquake with a specific character, the peak response can be different between a simplified and a detailed model.

(ii) The mass and stiffness distribution between the blades and the tower is important and directly effects the natural period of the structure.

(iii) It should be noted and emphasized that none of the results presented in this study may be taken to imply any direct or indirect consequence regarding the BÜRES turbine since the analyses are very preliminary and neither the geometry nor the boundary conditions nor the material properties are sufficiently known to reliably reflect the true conditions.

(iv) It is important to consider the tower as composed of shell elements during the analysis. Otherwise, the failure modes cause by local buckling can be missed.

(v) The three components of the earthquake was given to the FEM as input. The vertical component can also be critical. In some cases, the vertical component can cause a huge acceleration on the nacelle. This can cause huge forces on the top of the tower and at the base. Also the delicate equipment inside the nacelle can be damaged due to the high acceleration.

4.2. Future Work

(i) With regards to the importance of a detailed model of a wind turbine, a series of nonlinear time history analyses need to be conducted in order to observe the

importance of this model on the failure modes.

(ii) Comparisons need to be made between the time history results of the wind turbine subjected to two or three components of the earthquake in order to investigate the importance of the vertical component.

(iii) More ground motions with different characteristics need to be selected in order to evaluate the seismic response and capture the failure modes. There is a big gap between the PGA of the first chosen earthquake and the last one. Therefore, it is not possible to comment about the probability of failure of the wind turbine structure subjected to the base excitation. A wide range of earthquakes need to be chosen for this purpose.

APPENDIX A: Time-History Results of BÜRES Wind Turbine

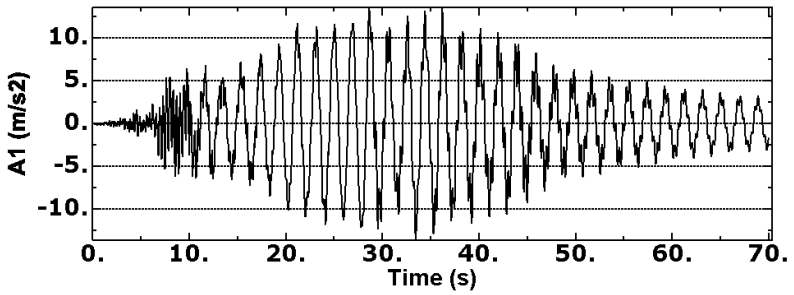

Figure A.1. Top acceleration in the horizontal x direction due to the amplified Landers record.

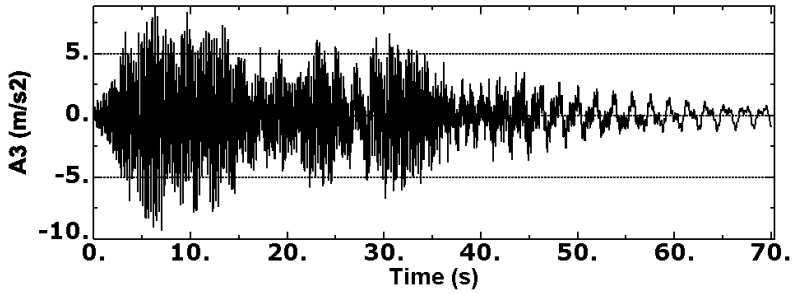

Figure A.2. Top acceleration in the horizontal z direction due to the amplified Landers record.

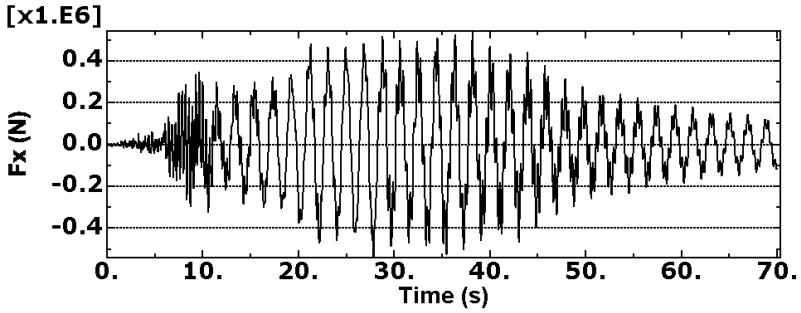

Figure A.3. Base shear in the horizontal x direction due to the amplified Landers record.

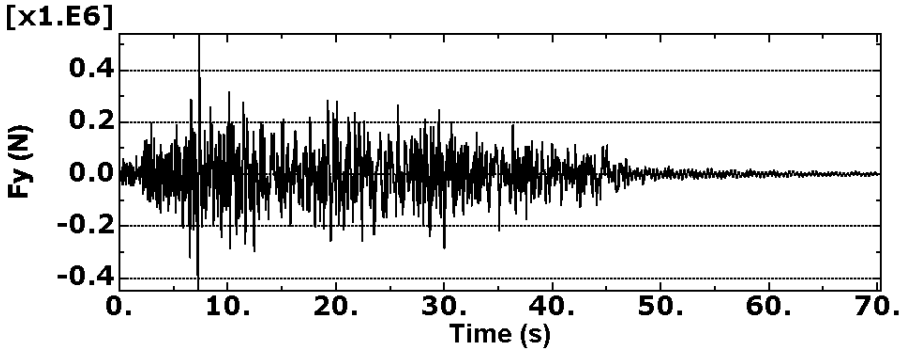

Figure A.4. Reaction force in the vertical direction due to the amplified Landers record.

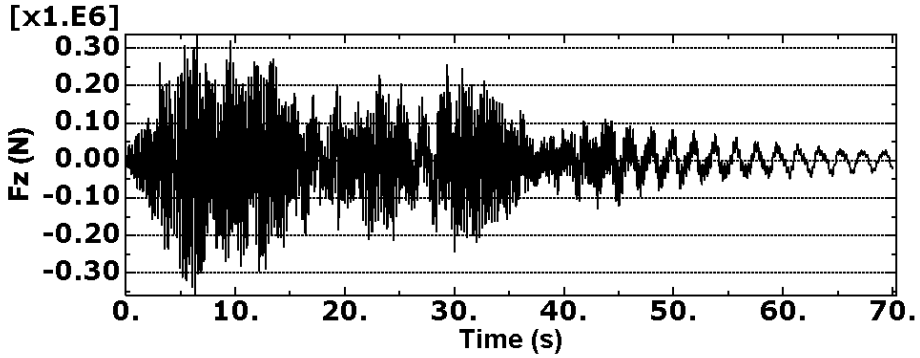

Figure A.5. Base shear in the horizontal z direction due to the amplified Landers record.

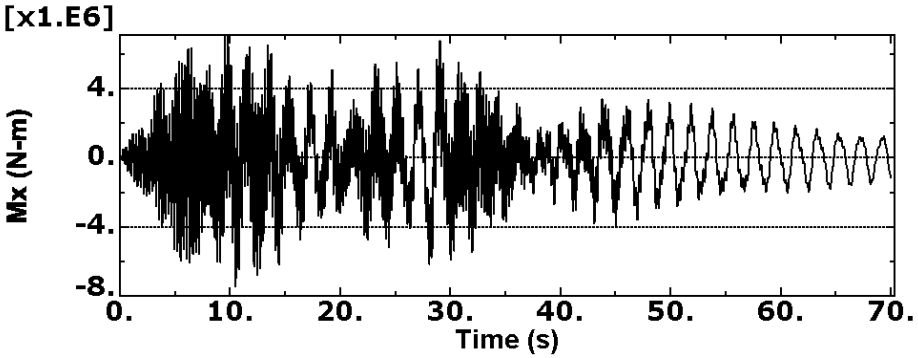

Figure A.6. Base moment with respect to the horizontal x axis due to the amplified Landers record.

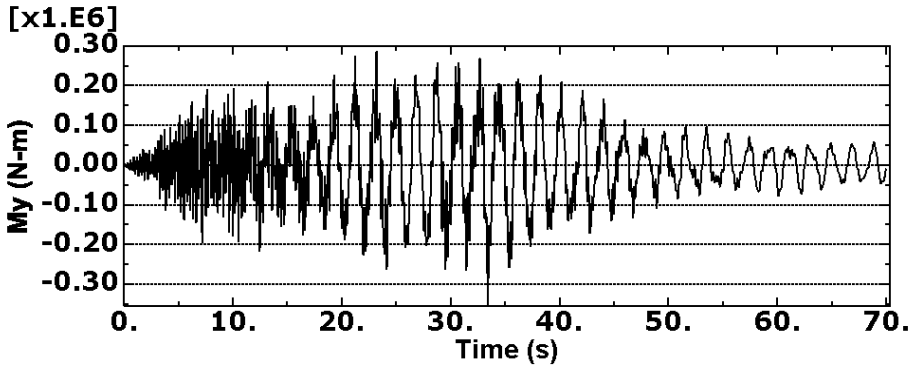

Figure A.7. Base moment with respect to the vertical axis due to the amplified Landers record.

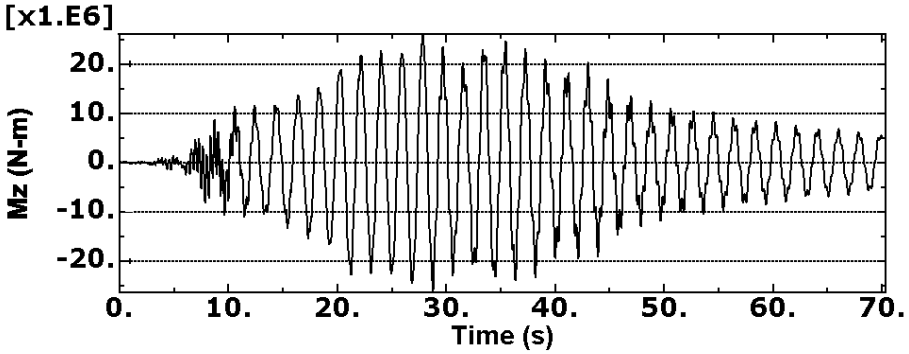

Figure A.8. Base moment with respect to the horizontal z axis due to the amplified Landers record.

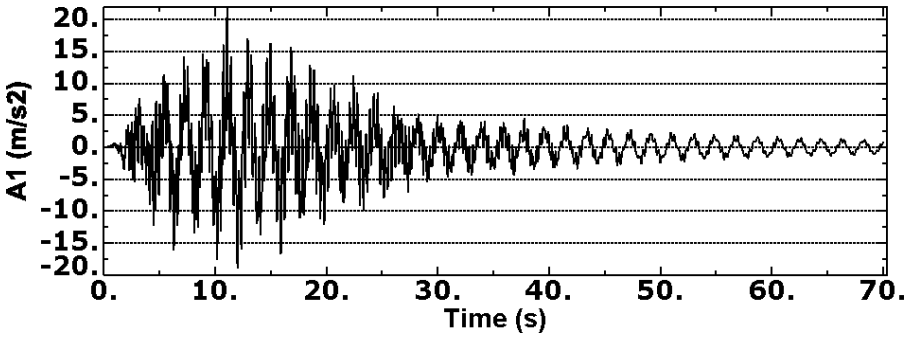

Figure A.9. Top acceleration in the horizontal x direction due to the amplified Imperial Valley 1940 record.

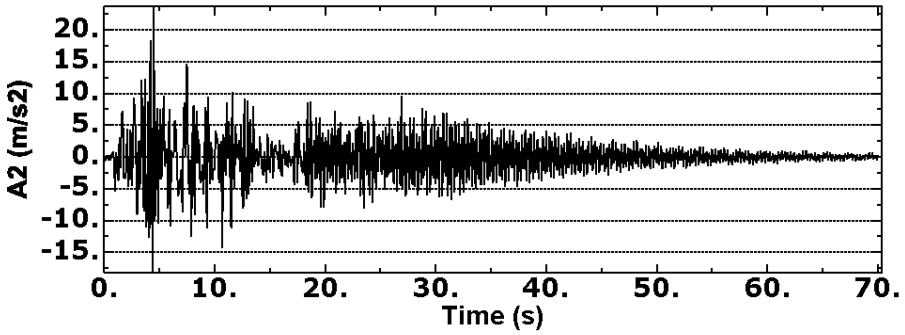

Figure A.10. Top acceleration in the vertical y direction due to the amplified Imperial Valley 1940 record.

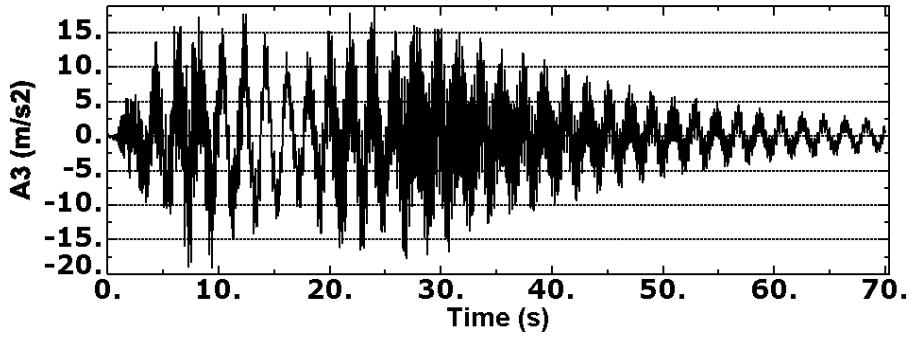

Figure A.11. Top acceleration in the horizontal z direction due to the amplified Imperial Valley 1940 record.

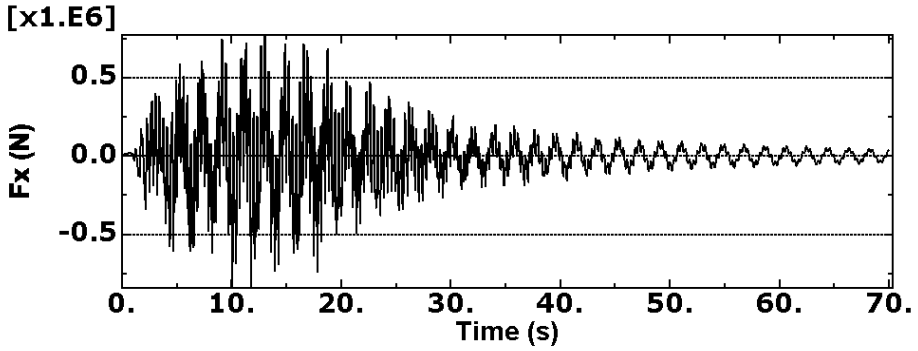

Figure A.12. Base shear in the horizontal x direction due to the amplified Imperial Valley 1940 record.

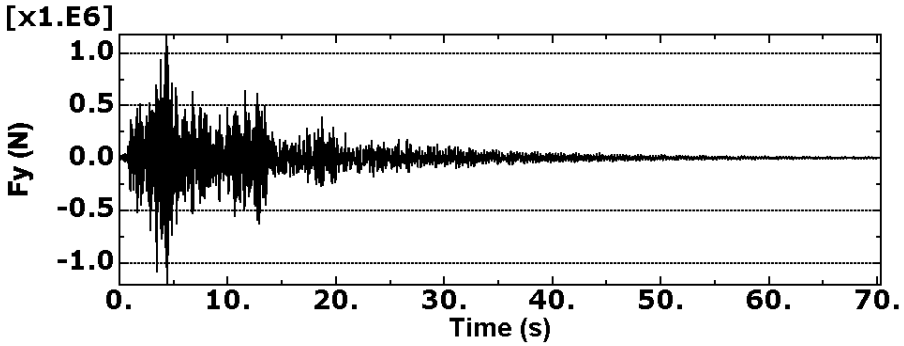

Figure A.13. Reaction force in the vertical direction due to the amplified Imperial Valley 1940 record.

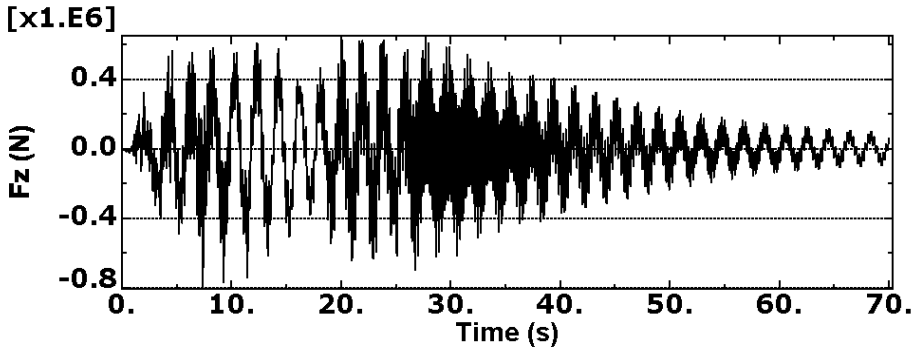

Figure A.14. Base shear in the horizontal z direction due to the amplified Imperial Valley 1940 record.

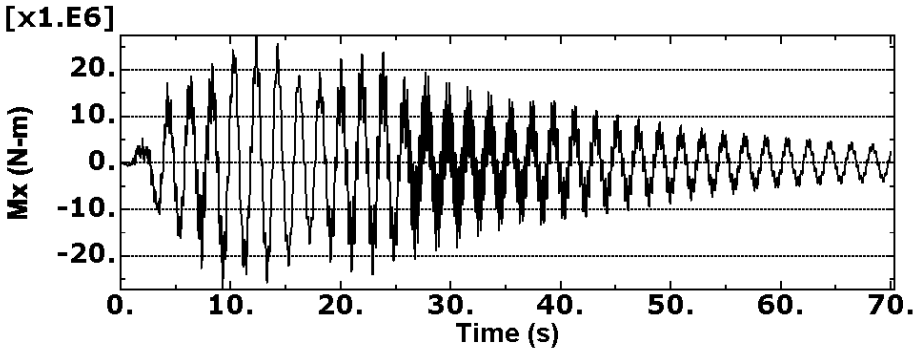

Figure A.15. Base moment with respect to the horizontal x axis due to the amplified Imperial Valley 1940 record.

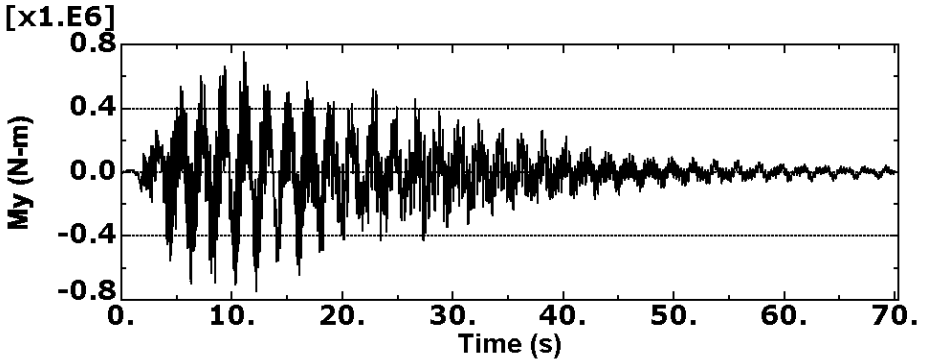

Figure A.16. Base moment with respect to the vertical y axis due to the amplified Imperial Valley 1940 record.

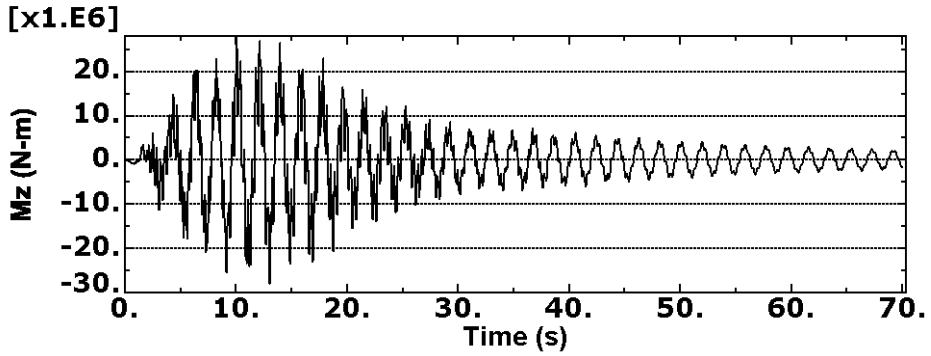

Figure A.17. Base moment with respect to the horizontal z axis due to the amplified Imperial Valley 1940 record.

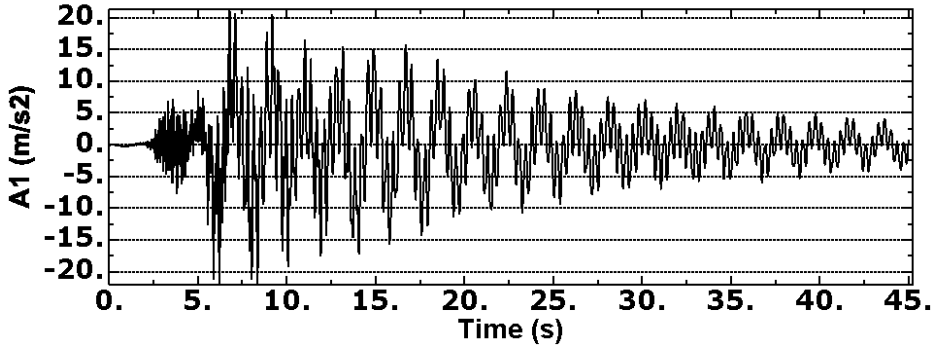

Figure A.18. Top acceleration in horizontal x direction due to the amplified Imperial Valley 1979 record.

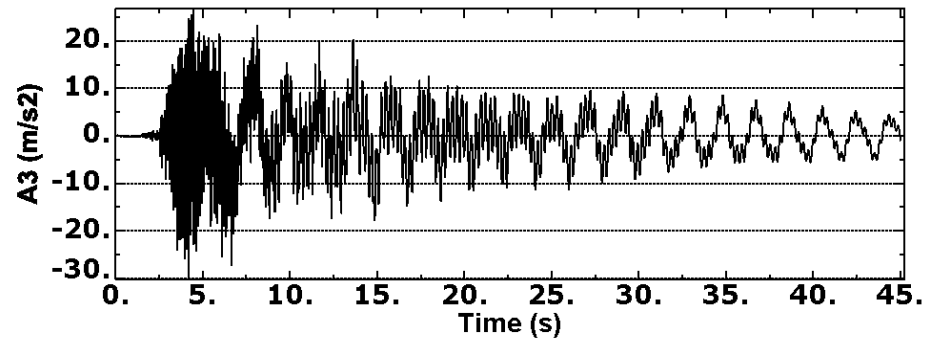

Figure A.19. Top acceleration in the horizontal z direction due to the amplified Imperial Valley 1979 record.

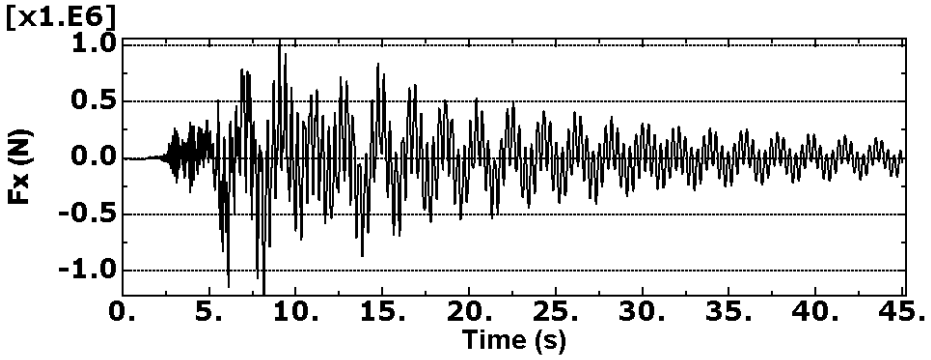

Figure A.20. Base shear in the horizontal x direction due the amplified Imperial Valley 1979 record.

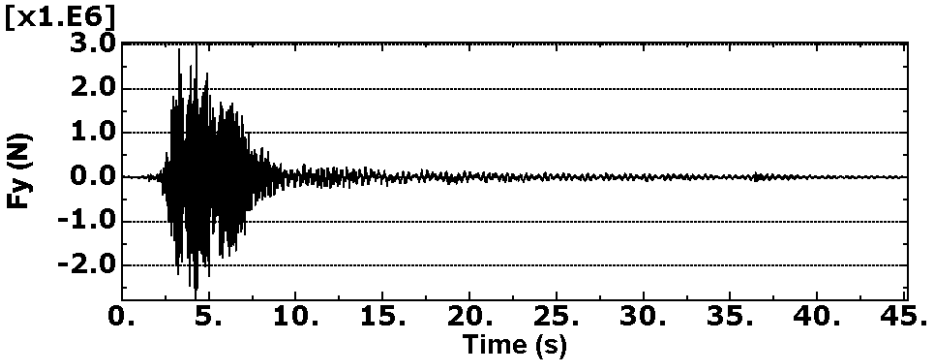

Figure A.21. Reaction force in the vertical direction due the amplified Imperial Valley 1979 record.

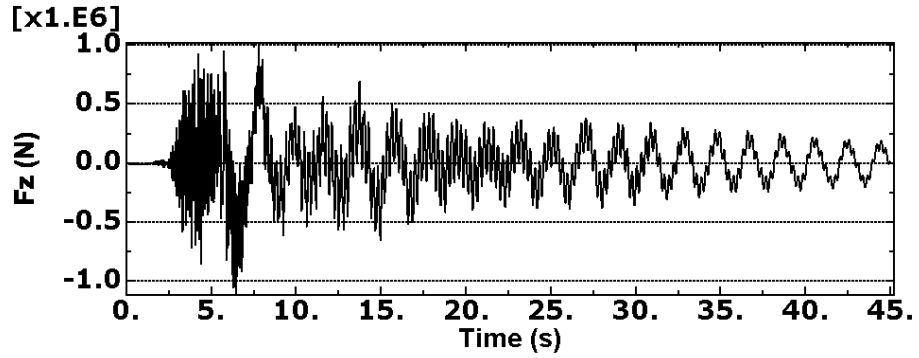

Figure A.22. Base shear in the horizontal z direction due the amplified Imperial Valley 1979 record.

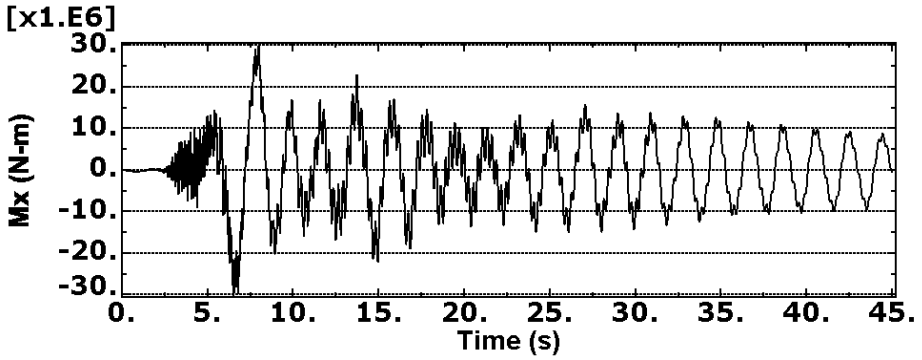

Figure A.23. Base moment with respect to the horizontal x axis due the amplified Imperial Valley 1979 record.

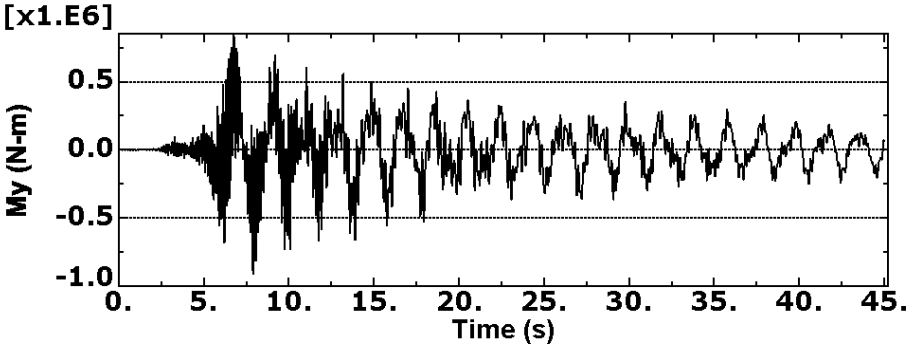

Figure A.24. Base moment with respect to the vertical y axis due the amplified Imperial Valley 1979 record.

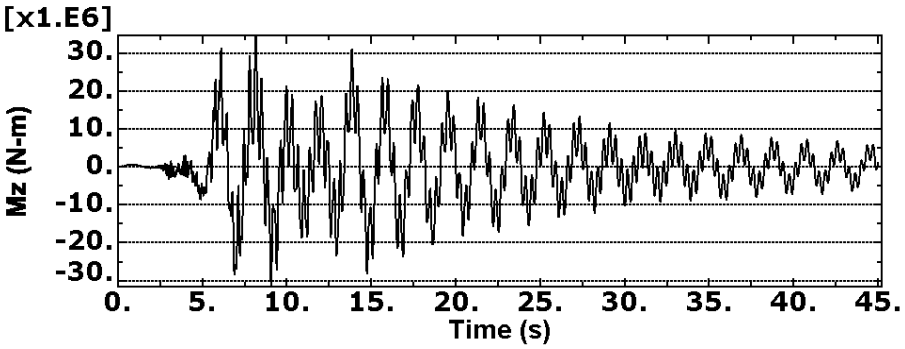

Figure A.25. Base moment with respect to the horizontal z axis due the amplified Imperial Valley 1979 record.

APPENDIX B: Response Spectras of the Ground Motions

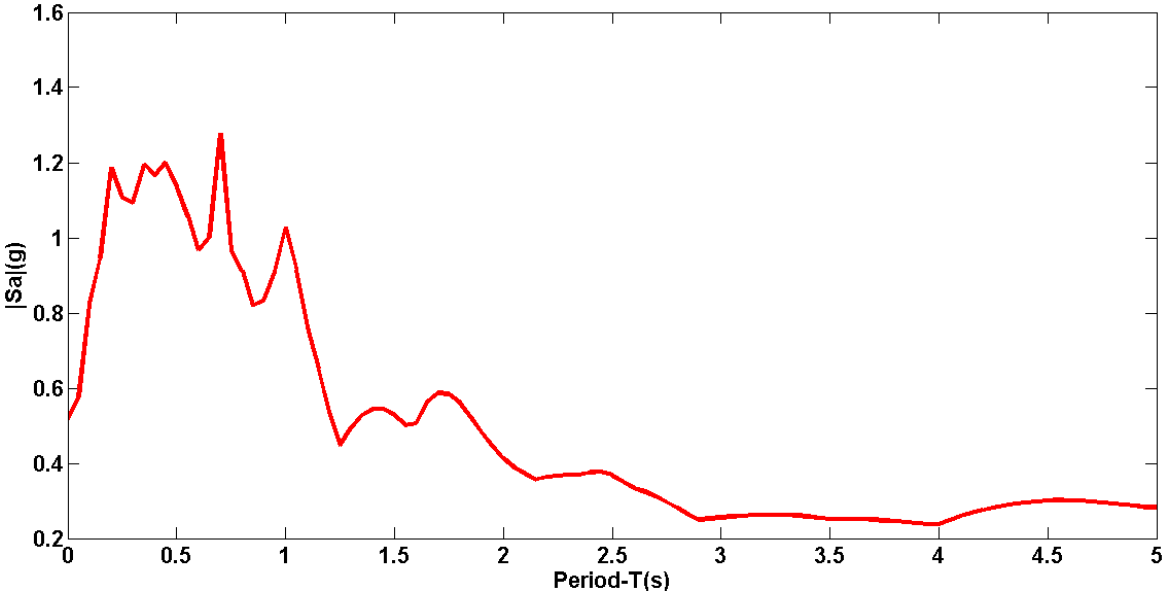

Figure B.1. Response spectra of the Imperial Valley record, N-S direction.

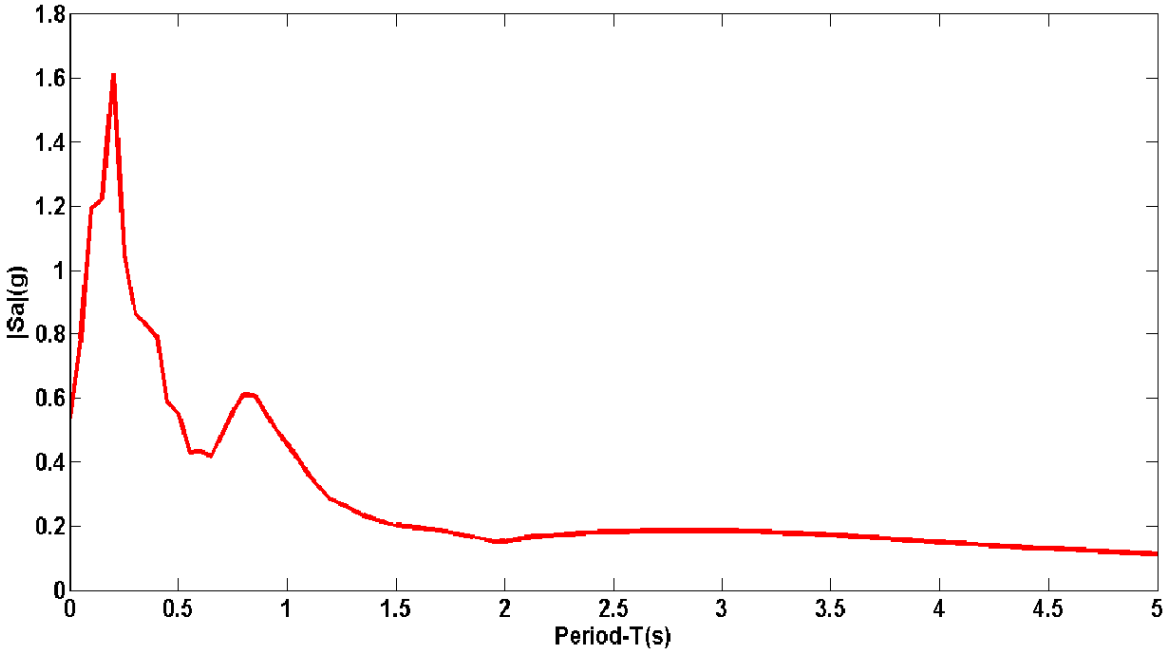

Figure B.2. Response spectra of the Imperial Valley record, vertical direction.

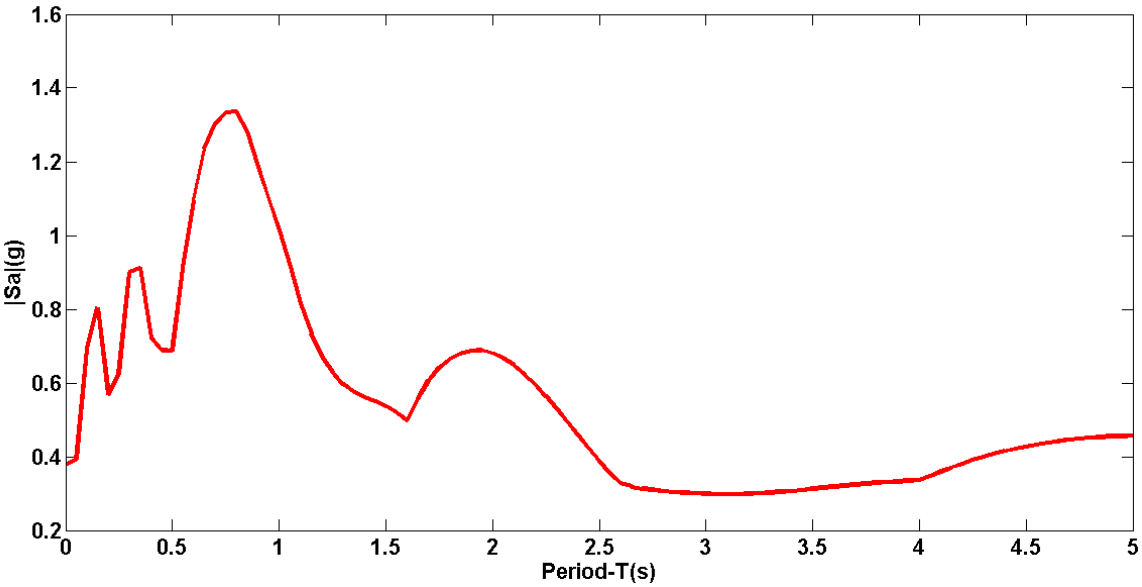

Figure B.3. Response spectra of the Imperial Valley record, E-W direction.

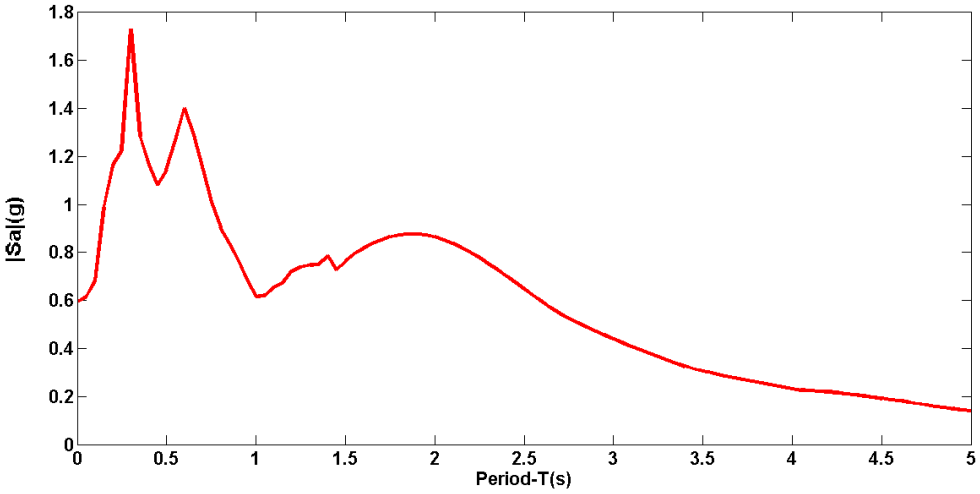

Figure B.4. Response spectra of the N.Palm Springs record, E-W direction.

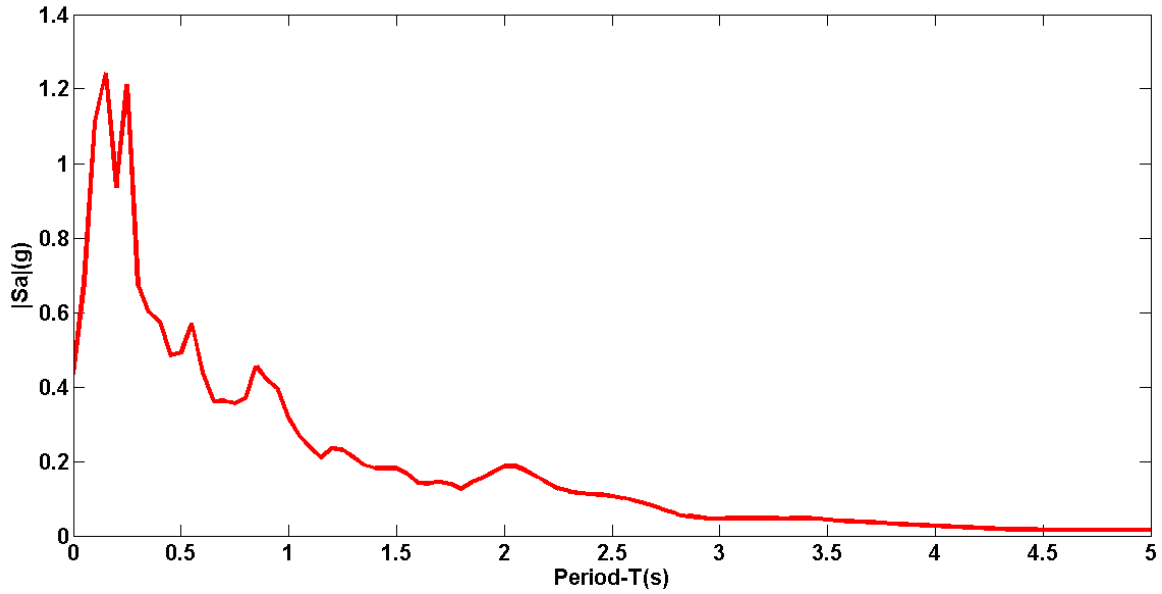

Figure B.5. Response spectra of the N. Palm Springs record, vertical direction.

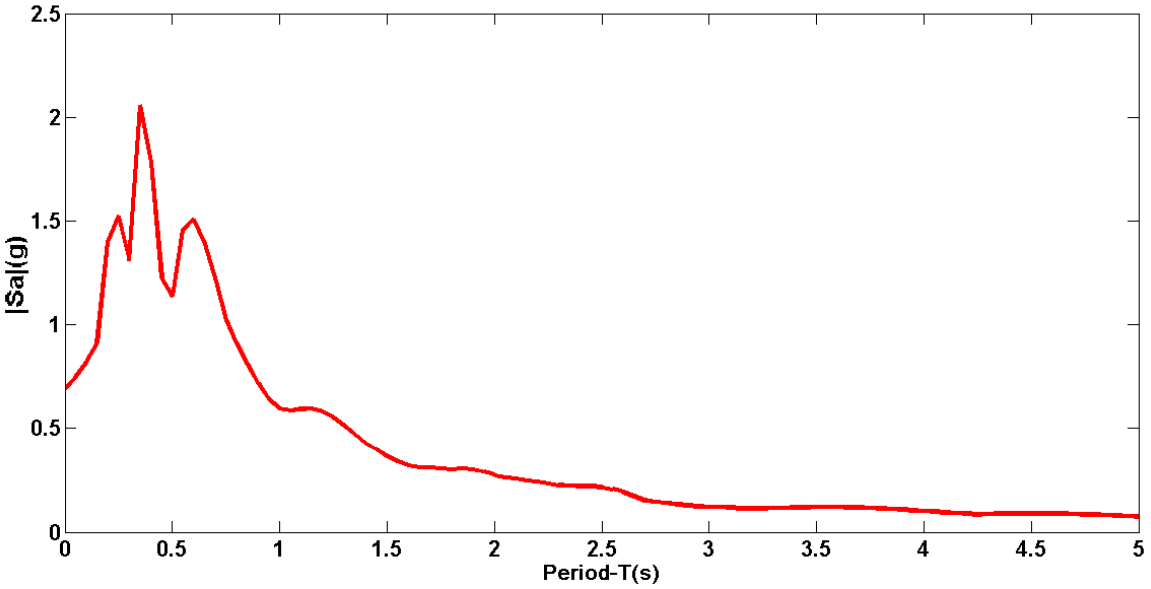

Figure B.6. Response spectra of the N. Palm Springs record, N-S direction.

REFERENCES

1. Prowell, I., M. Veletzos, A. Elgamal and J. Restrepo, "Shake Table Test of a 65 kW Wind Turbine and Computational Simulation", *14th World Conference on Earthquake Engineering, Beijing, China*, pp. 12–17, 2008.

2. Sim, H.-B., I. Prowell, A. Elgamal and C.-M. Uang, "Flexural Tests and Associated Study of a Full-Scale 65-kW Wind Turbine Tower", *Journal of Structural Engineering*, Vol. 140, No. 5, 2013.

3. Prowell, I., M. Veletzos, A. Elgamal and J. Restrepo, "Experimental and Numerical Seismic Response of a 65 kW Wind Turbine", *Journal of Earthquake Engineering*, Vol. 13, No. 8, pp. 1172–1190, 2009.

4. Prowell, I., A. Elgamal, C.-M. Uang, J. Enrique Luco, H. Romanowitz and E. Duggan, "Shake Table Testing and Numerical Simulation of a Utility-scale Wind Turbine Including Operational Effects", *Wind Energy*, 2013.

5. PEER, N., "Data Base", *Pacific Earthquake Engineering Research Center: Next Generation Attenuation Database [http://peer. berkeley. edu/nga/]: The Regents of the University of California*, 2005.

6. Association, E. W. E. and E. C. D.-G. for Energy, *Wind energy–the facts*, European Wind Energy Association, 1997.

7. Gökçek, M. and M. S. Genç, "Evaluation of Electricity Generation and Energy Cost of Wind Energy Conversion Systems (WECSs) in Central Turkey", *Applied Energy*, Vol. 86, No. 12, pp. 2731–2739, 2009.

8. Code, T. E., "Specifications for Buildings to Be Built in Seismic Areas", *Ministry of Public Works and Settlement. Ankara, Turkey (in Turkish)*, 2007.

9. Boyle, G., *Renewable Energy*, Oxford, 2004.

10. Hau, E. and H. Von Renouard, *Wind turbines: Fundamentals, Technologies, Application, Economics*, Springer, New York City, 2013.

11. Nijssen, R. P. L., "Fatigue Life Prediction and Strength Degradation of Wind Turbine Rotor Blade Composites", *Contractor Report SAND2006-7810P, Sandia National Laboratories, Albuquerque, NM*, 2006.

12. Veritas, N., *Guidelines for Design of Wind Turbines*, Roskilde, 2002.

13. WindEnergie, G.-L., *Guideline for the Certification of Wind Turbines*, Munich, 2003.

14. Agbayani, N. A., *A Technical Overview of ASCE/AWEA RP2011: Recommended Practice for Compliance of Large Land-based Wind Turbine Support Structures*, ASCE, 2014.

15. Committee, A., *Recommended Practice for Compliance of LargeLand-based Wind Turbine Support Structures*, Washington D.c., 2011.

16. Bazeos, N., G. Hatzigeorgiou, I. Hondros, H. Karamaneas, D. Karabalis and D. Beskos, "Static, Seismic and Stability Analyses of a Prototype Wind Turbine Steel Tower", *Engineering Structures*, Vol. 24, No. 8, pp. 1015–1025, 2002.

17. Lavassas, I., G. Nikolaidis, P. Zervas, E. Efthimiou, I. Doudoumis and C. Baniotopoulos, "Analysis and Design of the Prototype of a Steel 1-MW Wind Turbine Tower", *Engineering structures*, Vol. 25, No. 8, pp. 1097–1106, 2003.

18. Ishihara, T. and M. Sarwar, "Numerical and Theoretical Study on Seismic Response of Wind Turbines", *European Wind Energy Conference and Exhibition*, pp. 1–5, Brussels, 2008.

19. Ritschel, U., I. Warnke, J. Kirchner and B. Meussen, "Wind Turbines and Earth-

quakes", *2nd World Wind Energy Conference*, pp. 1–8, World Wind Energy Association Cape Town, South Africa, Wanda Vista, 2003.

20. Øye, S., "Flex 5 user manual", *Danske Techniske Hogskole*, 1999.

21. Nuta, E., C. Christopoulos and J. A. Packer, "Methodology for Seismic Risk Assessment for Tubular Steel Wind Turbine Towers: Application to Canadian Seismic Environment", *Canadian Journal of Civil Engineering*, Vol. 38, No. 3, pp. 293–304, 2011.

22. WindEnergie, G. L., *Guidelines for the Certification of Offshore Wind Turbines*, Hamburg, 2005.

23. Bossanyi, E., "GH bladed Theory Manual", *GH & Partners Ltd*, 2003.

24. Jonkman, J. M. and M. L. Buhl Jr, "FAST User's guide", *Golden, CO: National Renewable Energy Laboratory*, 2005.

25. Asareh, M. and I. Prowell, "Seismic Loading for FAST", *Contract*, Vol. 303, pp. 275–3000, 2011.

26. Witcher, D., "Seismic Analysis of Wind Turbines in the Time Domain", *Wind Energy*, Vol. 8, No. 1, pp. 81–91, 2005.

27. Mazzoni, S., F. McKenna, M. H. Scott, G. L. Fenves *et al.*, "OpenSees Command Language Manual", *Pacific Earthquake Engineering Research (PEER) Center*, 2006.

28. Prowell, I., A. Elgamal, C. Uang and J. Jonkman, "Estimation of Seismic Load Demand for a Wind Turbine in the Time Domain", *Report No. NREL/CP 500*, Vol. 47536, 2010.

29. Documentation, A., "ABAQUS Analysis User's Manual", *Materials. Other plasticity models. Concrete*, 2010.

30. Documentation, A. and U. Manual, "Version 6.12", *Simulia, Dassault Systèmes*, 2012.

31. Chopra, A. K., *Dynamics of Structures*, Vol. 3, Prentice Hall, New Jersey, 1995.

32. Somerville, P., "Development of an Improved Representation of Near Fault Ground Motions", *SMIP98 Seminar on Utilization of Strong-Motion Data*, Vol. 15, Oakland, California, 1998.